(NASA-CR-149302) THE SOLIDIFICATION UNDER ZERO GRAVITY CONDITIONS OF BINARY ALLOYS EXHIBITING SOLID STATE IMMISCIBILITY Final Report (Washington State Univ.) 88 p HC $5.00 CSCL 20I G3/76

N76-24041

Unclas 28091

WASHINGTON STATE UNIVERSITY 1890

COLLEGE OF ENGINEERING

RESEARCH DIVISION

FINAL REPORT

NASA Research Contract No. NAS8-29725

"The Solidification Under Zero Gravity Conditions of Binary Alloys Exhibiting Solid State Immiscibility"

by

A.A. Johnson, R.P. Anantatmula, R.J. Horylev, S.P. Gupta and R.S. Vatne

October 1, 1975

This report was prepared by the Department of Materials Science and Engineering, Washington State University, Pullman, WA 99163, under Contract NAS8-29725 for the George C. Marshall Space Flight Center of the National Aeronautics and Space Administration.

ABSTRACT

A detailed study of the solidification behavior of gold-silicon alloys containing up to 25 at. % silicon has been carried out and a mathematical model of gravity segregation during solidification has been developed. The purpose of this work was to provide a background of knowledge which can be used in the design of zero gravity solidification experiments to be carried out in the 300-' drop tower, in Aerobee rockets and in future space missions. Such experiments are needed to develop the basic scientific knowledge required for the design of economically viable space manufacturing processes. Some preliminary zero gravity experiments have been carried out on a gold-25 at. % silicon alloy using the drop tower facility.

TABLE OF CONTENTS

LIST OF TABLES

LIST OF FIGURES

1. INTRODUCTION

As the United States' space program has developed, numerous ideas for making use of the low or zero gravity environment in space for manufacturing new types of materials have been put forward.[1] In some manned space missions, demonstration experiments have been performed, and in the Skylab mission[2] an extensive series of materials science experiments were completed. The results of all of this work have tended to give credence to the idea that sooner or later it will be economically profitable to manufacture materials in space. The immediate effect, however, has been to provide results of basic scientific importance and to underline our ignorance of the role of the earth's gravitational field in terrestrial materials processing.

If the manufacture of materials in space is to become a reality, much research has to be carried out to establish the basic differences between materials processing with and without a gravitational field. Work in the terrestrial gravitational field can be carried out in a conventional laboratory and is not particularly expensive or time-consuming. Work under zero gravity conditions is much more difficult and expensive. Some work can be performed in manned space missions but, from a scientific point of view, other approaches can be at least as valuable. The 300-ft drop tower facility at the Marshall Space Flight Center provides zero gravity conditions for about 3.5 secs during free fall, and the current program of Aerobee rocket flights gives a working time of about six mins. Using such facilities, experiments can be repeated to establish their reproducibility more readily than in a manned space flight.

In this report we describe two years of work on one segment of NASA's program aimed at providing some of this basic knowledge needed to develop space processing techniques. Our part of the program has been concerned with binary alloy systems in which the components are miscible in the liquid state and immiscible in the solid state, and we have taken the gold-silicon system as a model for detailed study. It is particularly suitable because gold and silicon are both readily obtainable in a state of high purity and because in the earth's gravitational field there is a strong tendency for gravity segregation to occur during solidification as a result of the widely different specific gravities of gold and silicon. These two elements have very low mutual solubilities[3,4,5] and undergo a simple eutectic reaction. The eutectic temperature has been reported to be about 370°C.[6,7] Recent measurements of the eutectic composition have given 8.6 ±0.3 at. % silicon[8] and 17.9 at. % silicon.[9] Andersen et al.[9] have shown that quenched alloys near the eutectic composition contain a compound, Au_3Si, which has an orthorhombic structure. This compound undergoes a surface dissociation reaction at room temperature and a bulk dissociation reaction at higher temperatures. The excess gold appears in the form of submicron-diameter gold fibers threading the compound.

As the investigation proceeded over the past two years, some wrong turnings were taken and had to be retraced and some subsidiary topics were explored. A little work, for example, was carried out on the gold-germanium, silver-germanium and aluminum-silver systems. All of this activity is recorded in a series of twenty-five monthly reports. In this final report we concentrate on bringing together and integrating the most important parts of our work in a document of manageable propor-

tions. Readers interested in obtaining a more detailed account of our work should refer to the monthly reports and to the papers which we have published[10] or are in the process of publishing in the open literature.[11-13]

2. EXPERIMENTAL PROCEDURES

2.1 Specimen Preparation

The starting materials for all of the work described in this report were gold of 99.999% purity obtained from the Sigmund Cohn Corporation and silicon of 99.999995% purity obtained from the Research Inorganic/ Organic Chemical Corporation. The gold was in the form of 1-mm-diameter wire and the silicon in the form of polycrystalline lumps. Each alloy was prepared by weighing appropriate amounts of gold and silicon into a quartz tube which subsequently was evacuated and sealed. The sealed tube then was heated to about 650°C, shaken vigorously to ensure thorough mixing, held at temperature for about 15 minutes with intermittent further shaking and then quenched into cold water. The rod obtained in this way was approximately 6 mm in diameter. The procedures followed from this point on depended on whether the alloy was being prepared for terrestrial gravity experiments in the laboratory at Washington State University or drop tower experiments, with or without actually dropping the specimen, at the Marshall Space Flight Center in Huntsville, Alabama.

For the WSU laboratory experiments, specimens approximately 6 mm in length were cut from the rod. In each one a small hole about 3 mm deep was drilled into one end face to take a thermocouple. About 3 mm was removed from the top and the bottom of each ingot before specimens were cut from it so as to avoid possible inhomogeneity resulting from segre-

gation of proeutectic silicon. Each specimen was placed in a cylindrical tantalum capsule of 0.8-mm wall thickness with a cap and tube to carry the thermocouple. The cap was sealed onto the capsule using Saureisen, a proprietary ceramic cement. One of these specimen capsules is shown in Figure 1.

For the drop tower experiments a specimen capsule design was evolved through discussions in Huntsville with Mr. I. C. Yates and his colleagues. The type of specimen chosen consisted of a rectangular cross-section prism of dimensions 1.27 x 0.63 x 0.32 cm. The capsule consisted of three parts and these are shown in an exploded view in Figure 2. First there was the body of the capsule which was machined from tantalum. Secondly, there was the base plate, also machined from tantalum and designed so that it could be electron-beam-welded onto the body of the capsule, thereby sealing off one face. Thirdly, there was the top plate, again of tantalum, containing a hole through which was mounted a sealed tantalum tube containing the thermocouple. This also could be electron-beam-welded onto one face of the capsule so as to completely seal the capsule.

To seal one of these capsules with a gold-silicon alloy inside, the following procedures were adopted. First a base plate was welded onto one of the capsule bodies and an appropriate quantity of the molten alloy was poured into the capsule so that it was essentially filled. Then, when solidified, the specimen was removed from this first tantalum capsule by cutting away the capsule. It then was drilled to take the thermocouple tube and mounted in another capsule in which the base plate already was welded into position. Then the top plate with the thermocouple was placed in position and the final weld was made to seal the

capsule in readiness for use. Although this process was extravagant in its use of the capsules, it was found that this was worthwhile because it resulted in success almost every time. The electron beam welding was carried out at the Battelle-Northwest Laboratories in Richland, Washington under a subcontract from Washington State University.

2.2 Terrestrial Gravity Solidification Experiments

To carry out a laboratory solidification experiment at WSU the specimen and capsule assembly first was mounted rigidly in a vertical position. A vertical tube furnace tnen was put around it by raising the furnace from underneath. Before being placed into position the furnace was brought to the desired equilibration temperature, which was in most cases at or close to 650°C. The specimen then was equilibrated in the furnace, usually for about 20 minutes, and then the furnace was removed in order to solidify the specimens. Some specimens were allowed to cool in air, while others were quenched into brine, cold water or oil. In some instances where a particularly low cooling rate was required, the specimen was allowed to cool in the furnace before the furnace was removed. The cooling rate was obtained by feeding a signal from a calibrated thermocouple to a chart recorder and recording the temperature of the specimen as a function of time. The cooling rate was taken to be the temperature interval between the liquidus and the eutectic divided by the time to achieve cooling through this range. After solidification, the specimen was removed from the capsule and mounted in a cold-setting plastic. It then was polished with several successively finer grades of silicon carbide papers and two grades of aluminum powder on rotating polishing wheels. In each case a longitudinal section through the center of the specimen was studied.

2.3 Zero Gravity Drop Tower Experiments

For the drop tower experiments the instrument package for solidification studies developed by J. L. Reger of the TRW Laboratories in Redondo Beach, California was used.[14] In this facility the specimen is mounted inside the coils of a small resistance-heated furnace. The specimen is brought to equilibrium at the required temperature by adjusting the current through the furnace, and cooling is achieved by a jet of water driven by a cylinder of compressed gas and delivered through a specially designed nozzle. Details of this system have been described elsewhere. The heating and cooling cycle could be carried out either in terrestrial gravity or with the instrument package in free fall in the drop tower. The 300-ft drop distance provided a time of about 3.5 secs during which the gravitational field was no more than 10^{-5} g. During free fall the thermocouple signal was transmitted to a block tower and recorded using a telemetering system.

When a specimen had been processed through the drop tower facility it was taken out of its tantalum capsule and, initially, each of its six surfaces was polished for examination. When the outside surfaces had been studied, transverse and longitudinal sections through the center of the specimen also were examined.

2.4 X-Ray Diffraction Techniques

X-ray diffraction traces were obtained for each solidified specimen using CuK_α radiation and a nickel filter. In addition, some work was done on one drop tower specimen using a micro-diffraction technique developed by Sorem. In this method the specimen surface was scratched with a fine tungsten stylus prepared by electropolishing. This created

a small amount of powder from an easily recognizable region of the specimen. The scratching and generation of powder were carried out under a stereomicroscope so that there was good control over the region which was scratched. In this way a material containing two or more phases could be studied and diffraction patterns could be obtained from each phase. The powder from a given scratch was picked up by taking a fine gelatin fiber wetted in water and rubbing it in the powder. This fiber with its powder specimen then was mounted in a 57.3mm Debye-Scherrer camera and a diffraction pattern obtained using CuK_{α} radiation and a nickel filter.

2.5 Scanning Electron Microscopy Techniques

Each specimen was studied extensively using an ETEC scanning electron microscope. This was found to be an extremely powerful technique, since the specimen could be placed in the specimen chamber and micrographs of it covering a wide range of magnifications could be obtained in rapid succession. A low-magnification micrograph covering the entire surface was obtained for most specimens and then the magnification was increased in steps and the structure at various magnifications documented. The instrument was used mostly in the backscattered-electron mode of operation, since this tended to give the best contrast. Some work was done using the secondary-electron mode of operation, but all of the micrographs reported in this document were obtained using the backscattered-electron technique. In general, it was found more convenient to use the scanning electron microscope than to use a metallograph, and so much of the work usually done with optical microscopy was in this case carried out with scanning electron microscopy. Because of the relatively

high conductivity of all of the phases studied, it was not found necessary to coat the specimens with a conductor.

2.6 Electron Beam Microprobe Analysis Technique

A limited amount of work was carried out on drop tower specimens using an ARL electron beam microprobe analyzer. The instrument used was located at the University of Idaho and was operated by Professor Charles Knowles, to whom the authors are greatly indebted. The specimens were used in an uncoated condition and both point counts and the traverses were used for analyzing the phases present in solidified specimens. There were some problems using this technique because there are no standards containing both silicon and gold. We found in general that the best approach was to use a specimen known to contain Au_3Si as the standard.

3. MATHEMATICAL THEORY OF GRAVITY SEGREGATION

3.1 Initial Assumptions

The most pronounced gravity segregation effects in the gold-silicon system occur on the silicon-rich side of the eutectic composition. When a hypereutectic alloy is cooled from above the liquidus temperature, small, irregular faceted silicon crystals are rejected from the melt. These tend to rise to the surface of the melt and, by the time the alloy solidifies at the eutectic temperature, partial or total segregation of the particles has occurred. It was found early in the investigation that, working with a gold-25 at. % silicon alloy, for cooling rates above about 120°C sec^{-1} the segregation is negligible, while for cooling

rates below about 10° sec^{-1} it is essentially complete for the type of specimens used in this investigation. Since this range of cooling rates, i.e., from 10 to 120°C sec^{-1}, is easily obtainable in the laboratory, it was decided to make a thorough study of gravity segregation in this alloy and to try to develop a mathematical model to describe it.

Gravity segregation in a solidifying alloy is a complex phenomenon, and simplifying assumptions necessarily must be made to make the problem tractable. We have been guided in making our initial assumptions by the results of preliminary experiments. The assumptions with which we shall start out are:

1. The silicon particles are all nucleated at the instant the temperature reaches the liquidus temperature, T_{ℓ}.
2. Quasi-chemical equilibrium is maintained as cooling proceeds below the liquidus temperature.
3. Complete solidification occurs at the eutectic temperature, T_e.
4. The liquidus line between the eutectic composition, C_e, and the alloy composition, C', can be represented by a straight line joining one point representing the eutectic composition and temperature and another representing the alloy composition and the liquidus temperature at that composition.
5. Between the liquidus and eutectic temperatures the liquid alloy viscosity, η, can be regarded as constant. (This is a fairly drastic assumption and its consequences are explored in Section 3.5.)
6. Viscosity and density changes in the liquid alloy caused by composition changes resulting from the rejection of primary silicon during solidification can be neglected.

7. From a hydrodynamic point of view, the irregular faceted silicon crystals can be treated as spheres of equivalent volume.

For the time being, we simply state what our assumptions are. Later we shall discuss in the light of our experimental work the extent to which they may be invalid.

3.2 Formulation of the Problem

Imagine that a specimen is being cooled from a temperature above T_ℓ. When it reaches T_ℓ, silicon particles will be nucleated in the melt and there will be, say, n particles per unit volume. As the temperature is lowered to T_e, each particle will grow to some maximum value reached at T_e where the entire melt solidifies, thus terminating the growth. Suppose that the cooling rate between T_ℓ and T_e is R°C sec^{-1} and that $t = o$ when $T = T_\ell$. We now can calculate the particle radius, $\underline{a}$, as a function of time.

At a temperature T between T_ℓ and T_e the composition of the equilibrium liquid phase changes by an amount which, from Figure 3, is given by

$$\tan \Theta = \frac{T_\ell - T_e}{C' - C_e} = \frac{T_\ell - T}{C' - C}$$

i.e.,

$$C' - C = \Delta C = \frac{(C' - C_e)(T_\ell - T)}{T_\ell - T_e} \qquad (1)$$

This means that, for every 100 atoms of the original liquid alloy, ΔC atoms will be rejected from solution at a temperature T. If 1 cm^3 of

the liquid alloy contains N atoms, then, at a temperature T, 1 cm^3 of the liquid will reject $\frac{N\Delta C}{100}$ atoms. If there are n particles, each particle will contain $\frac{N\Delta C}{100}$ atoms. Thus, if m_{Si} is the mass of one silicon atom and ρ_{Si} is the density of silicon, we can say that the volume, V, of each silicon particle is

$$V = \frac{4}{3}\pi a^3 = \frac{N\Delta C\, m_{Si}}{100n\, \rho_{Si}} \tag{2}$$

or $$a = \sqrt[3]{\frac{3N\Delta C\, m_{Si}}{4\pi\, 100n\, \rho_{Si}}} = \sqrt[3]{\frac{3N(C' - C_e)(T_\ell - T)m_{Si}}{400\pi\, n\, \rho_{Si}(T_\ell - T_e)}} \tag{3}$$

Thus we have an equation relating the radius of a rejected particle to the temperature. We now need to convert this to an equation relating the radius to the time.

At a time t, the temperature T is given by

$$Rt = (T_\ell - T) \tag{4}$$

which, by substitution in equation (3), yields

$$a = \sqrt[3]{\frac{3N(C' - C_e)Rm_{Si}\, t}{400\pi\, n\, \rho_{Si}\, (T_\ell - T_e)}} \tag{5}$$

Alternatively, if we are interested in the variation of the volume of the particle with time, we may write

$$V = \frac{N(C' - C_e)Rm_{Si}\, t}{100n\, \rho_{Si}(T_\ell - T_e)} \tag{6}$$

Thus the particle volume increases linearly with time. For a given composition we may write

$$V = At \tag{7}$$

where

$$A = \frac{N(C' - C_e)Rm_{Si}}{100n\,\rho_{Si}(T_\ell - T_e)} \tag{8}$$

We can now proceed to set up an equation of motion for an individual particle using Newton's third law of motion. This must be done with care, since we are dealing with a problem in which the particle mass varies with time. This type of problem has been discussed at length by Sommerfield[15] and others. The correct formulation is

$$\frac{d}{dt}\left(m(t)\,\frac{dy}{dt}\right) = F_b - F_d$$

or

$$m(t)\,\frac{d^2y}{dt^2} + \frac{dm(t)}{dt}\cdot\frac{dy}{dt} = F_b - F_d \tag{9}$$

where $m(t)$ is the mass of the particle which, like the volume, increases linearly with time; F_b is the buoyancy force acting on the particle, and F_d is the hydrodynamic drag force. F_b is given simply by

$$F_b = V(t)(\rho_l - \rho_{Si})g \tag{10}$$

where ρ_l is the density of the liquid alloy which, to a good approximation, can be regarded as independent of time. F_d is given by the Stokes' equation as

$$F_d = 6\pi\eta\, a(t)\frac{dy}{dt} \tag{11}$$

where η is the viscosity of the liquid alloy. Combining equations (5), (7), (9), (10) and (11) and rearranging, we obtain

$$\frac{d^2y}{dt^2} + t^{-1}\frac{dy}{dt} + Bt^{-2/3}\frac{dy}{dt} = C \tag{12}$$

where

$$B = \frac{6\pi\eta\sqrt[3]{\frac{3}{4\pi}}}{\rho_{Si}A^{2/3}} \tag{13}$$

$$C = \frac{(\rho_l - \rho_{Si})g}{\rho_{Si}} \tag{14}$$

We shall show below that B can have values ranging from about 5×10^4 to 1×10^8. The term $t^{-1}dy/dt$ in equation (12) is therefore very much smaller than the term $Bt^{-2/3}\, dy/dt$ and can be dropped. This leaves us with the problem of solving the equation

$$\frac{dy^2}{dt^2} + Bt^{-2/3}\frac{dy}{dt} + C \tag{15}$$

3.3 Mathematical Solution of the Problem

We can solve equation (15) by making the substitution

$$\frac{dy}{dt} = z, \text{ or } \frac{d^2y}{dt^2} = \frac{dz}{dt} \tag{16}$$

Making the substitution and multiplying through by $\exp(3Bt^{1/3})$, we obtain

$$\exp(3Bt^{1/3})\,\frac{dz}{dt} + B\exp(3Bt^{1/3})\,.\,t^{-2/3}z = C\exp(3Bt^{1/3})$$

or

$$\frac{d}{dt}\left[z\exp(3Bt^{1/3})\right] = C\exp(3Bt^{1/3})$$

which gives

$$z\exp(3Bt^{1/3}) = \int C\exp(3Bt^{1/3})dt + K_1 \qquad (17)$$

where K_1 is a constant of integration. We now have to evaluate the integral on the right-hand side of equation (17).

Let us make the substitution

$$t^{1/3} = l \qquad (18)$$

Then

$$\frac{1}{3}t^{-2/3}\,dt = dl$$

and

$$I = \int C\exp(3Bt^{1/3})dt = \int C\exp(3Bl)\cdot 3l^2 dl$$

$$= 3C\left[\frac{l^2\exp(3Bl)}{3B} - \int\frac{\exp(3Bl)}{3B}\cdot 2l\,dl\right]$$

$$= 3C\left[\frac{l^2\exp(3Bl)}{3B} - \frac{2}{3B}\left\{\frac{l\exp(3Bl)}{3B} - \int\frac{\exp(3Bl)}{3B}\,dl\right\}\right]$$

$$= 3C\left[\frac{l^2\exp(3Bl)}{3B} - \frac{2}{3B}\left\{\frac{l\exp(3Bl)}{3B} - \frac{\exp(3Bl)}{9B^2}\right\}\right]$$

or

$$I = 3C\exp(3Bl)\left[\frac{l^2}{3B} - \frac{2l}{9B^2} + \frac{2}{27B^3}\right] \qquad (19)$$

Substituting this expression for I into equation (17) gives

$$z = 3C\left[\frac{t^{2/3}}{3B} - \frac{2t^{1/3}}{9B^2} + \frac{2}{27B^3}\right] + K_1 \exp(-3Bt^{1/3})$$

$$= C\left[\frac{t^{2/3}}{B} - \frac{2t^{1/3}}{3B^2} + \frac{2}{9B^3}\right] + K_1 \exp(-3Bt^{1/3}) \qquad (20)$$

Going back to our original substitution, $z = \frac{dy}{dt}$, equation (16), we see that to obtain a solution for y we must solve the equation

$$y = \int C\left[\frac{t^{2/3}}{B} - \frac{2t^{1/3}}{3B^2} + \frac{2}{9B^3}\right] dt + \int K_1 \exp(-3Bt^{1/3})dt + K_2 \qquad (21)$$

where K_2 is another constant of integration. Carrying out the integrations, we obtain

$$y = \frac{C}{B}\left[\frac{3}{5}t^{5/3} - \frac{t^{4/3}}{2B} + \frac{2t}{9B^2}\right] - K_1\left[\frac{t^{2/3}\exp(-3Bt^{1/3})}{B} + \right.$$

$$\left. + \frac{2}{B}\left\{\frac{t^{1/3}\exp(-3Bt^{1/3})}{3B} + \frac{\exp(-3Bt^{1/3})}{9B^2}\right\}\right] + K_2 \qquad (22)$$

making use of the result of equation (19) to evaluate the second integral.

The constants K_1 and K_2 in equation (22) can be evaluated using the boundary conditions

$$\left.\begin{array}{l} y = 0 \text{ at } t = 0 \\ \\ \frac{dy}{dt} = 0 \text{ at } t = 0 \end{array}\right\} \qquad (23)$$

Inserting the first boundary condition into equation (22) gives

$$0 = -K_1 \cdot \frac{2}{B} \cdot \frac{1}{9B^2} + K_2$$

or

$$K_2 = \frac{2}{9B^3} K_1 \tag{24}$$

Inserting the second boundary condition into equation (20) gives

$$0 = \frac{2C}{9B^3} + K_1$$

or

$$K_1 = \frac{2C}{9B^3} \tag{25}$$

Substituting this value of K_1 into equation (24) gives

$$K_2 = \frac{-2}{9B^3} \cdot \frac{2C}{9B^3}$$

or

$$K_2 = \frac{-4C}{81B^6} \tag{26}$$

Thus our final solution is

$$y = \left[\frac{C}{B}\frac{3}{5}t^{5/3} - \frac{t^{4/3}}{2B} + \frac{2t}{9B^2}\right] + \frac{2C}{9B^4}\left[t^{2/3}\exp(-3Bt^{1/3}) + \right.$$
$$\left. + \frac{2t^{1/3}\exp(-3Bt^{1/3})}{3B} + \frac{2\exp(-3Bt^{1/3})}{9B^2}\right] - \frac{4C}{81B^6} \tag{27}$$

3.4 Simplification of the Solution

The solution represented by equation (27) is fairly complex and it is therefore appropriate to look at it term by term to find out whether any of the terms are small enough to be dropped. We note that the constant B contains the cooling rate R, whereas C is independent of R. We therefore must calculate B for a range of cooling rates embracing all

values likely to be studied experimentally. To carry through these calculations, we need to adopt values for the various quantities included in B, including the constant A which is given by equation (8) and in which the dependence of B on R resides.

The value of N, the number of atoms per cm^3 in the liquid alloy, can be calculated as follows. The lattice parameter of solid gold is 4.08Å and hence the volume of a unit cell is 67.9×10^{-24} cm^3. Each unit cell contains 4 atoms.

$\therefore$ No. of atoms per cm^3 for solid gold $= \dfrac{4}{67.9 \times 10^{-24}} = 5.89 \times 10^{22}$

Silicon has eight atoms per unit cell, a lattice parameter of 5.43Å and a unit cell volume of 160.1×10^{-24} cm^3.

$\therefore$ No. of atoms per cm^3 for solid silicon $= \dfrac{8}{160.1 \times 10^{-24}} = 5.00 \times 10^{22}$

Suppose that 1 cm^3 of the solid Au-25 at. % Si alloy contains 0.25x atoms of Si and 0.75x atoms of Au.

Since

$$0.25x \text{ atoms of silicon occupy } \frac{.25x}{5 \times 10^{22}} \text{ cm}^3$$

and

$$0.75x \text{ atoms of gold occupy } \frac{.75x}{5.89 \times 10^{22}} \text{ cm}^3$$

we have

$$\left(\frac{.25x}{5.00} + \frac{.75x}{5.89}\right) \times 10^{-22} = 1$$

which gives

$$x = 5.64 \times 10^{22} \text{ atoms cm}^{-3}$$

Thus the solid alloy contains 5.64×10^{22} atoms cm^{-3} at room temperature. Now, a gold alloy rich in gold typically expands about five percent in

melting. We therefore must subtract about five percent from the value of x to obtain N, the number of atoms per unit volume in the liquid alloy. This gives a value of N equal to 5.86×10^{22} atoms cm^{-3}.

The value of C' is of course 25 at. % and the value of C_e is 19.0 at. %. Thus $(C' - C_e)$ is equal to 6.0 at. %. The value of m_{Si} is 28.09 divided by Avogadro's number (6.023×10^{23}), which is 4.66×10^{-23} gram $atom^{-1}$. The value of ρ_{Si} is 2.33 gram cm^{-3}.

A value of n, the number of silicon particles per cm^3, can be derived only from experimental results. To do so, we must make use of a relationship between n on the one hand and the number of particles in a unit area of a two-dimensional section, N_a, and the number of particles intersected by a unit straight line in such a section, N_L, on the other. We shall use the expression for spherical particles as an approximation, since in fact our particles are irregular-faceted crystals. This expression is[16]

$$n = \frac{N_a^2}{2 N_L} \tag{28}$$

Values of N_a and N_L were obtained by preliminary measurements on three micrographs from each of two specimens. The values obtained using these values of N_a and N_L are shown in Table I. The average value of n from these six measurements is 12.3×10^6 particles cm^{-3}. It will be seen from Table I that there is some evidence that n varies with R, a point which will be taken up later.

The value of T_ℓ, the liquidus temperature at 25 at. % Si, was taken from the paper by Gerlach and Goel[7] to be 560°C. The eutectic temperature is close to 363°C. A value of 197°C therefore was used for $(T_\ell - T_e)$.

The density of the liquid alloy increases slightly as solid silicon is rejected from it and its silicon content falls from 25 to 19.0 at. %. Any value that we use is therefore an approximation at best. Since Au and Si atoms occupy comparable volumes in the pure solid phases, it was assumed that a reasonable value would be obtained by taking a weighted average of the densities of solid Au and solid Si, the weighting being carried out according to the relative atomic percentages of the two elements. Using the eutectic composition, this gives a value of 16.26 grams cm^{-3}. This value is probably a few percent in error, because no account has been taken of the volume change on melting and because of the uncertainty which exists concerning the basic assumption on which the estimate rests.

As far as the authors are aware, no viscosity measurements have been carried out on liquid gold-silicon alloys. The nearest measurements are those of Polk and Turnbull[17] on an alloy containing 77.8 at. % Au, 13.8 at. % Ge and 8.4 at. % Si. They found that the viscosity of this alloy was 11.5 centipoise at 406°C and 10.6 cp at 448°C. In the absence of any better values, a value of 10.0 centipoise was taken for our Au-25 at. % Si alloy. It seems unlikely that this will be in error by more than, say, ±20 percent. It is true, of course, that the viscosity is a function of temperature and so, again, there seems to be room for a further refinement of the theory in the future to take account of this.

Using all of these numerical values, and of course a value of 980 cm sec^{-2} for g, the constants A and B were calculated using values of R from 10^{-2} to 10^{3}°C sec^{-1}. The results of these calculations are shown in Table II. A and B are expressed in c.g.s. units. The constant C is independent of R and has a value of 5.78×10^{3} c.g.s. units.

Let us now take the smallest value of B, i.e., the one for R = 1000°C sec^{-1}, and insert it, together with the value for C, into equation (27). We obtain

$$y = \frac{5.78 \times 10^3}{5.65 \times 10^4}\left[\frac{3}{5}t^{5/3} - \frac{t^{4/3}}{11.30 \times 10^4} + \frac{2t}{2.87 \times 10^{10}}\right]$$

$$+ \frac{1.16 \times 10^4}{9.17 \times 10^{19}}\left[t^{2/3}\exp(-1.69 \times 10^5 t^{1/3}) + \frac{2t^{1/3}\exp(-1.69 \times 10^5 t^{1/3})}{1.69 \times 10^5} + \right.$$

$$\left. + \frac{2\exp(-1.69 \times 10^5 t^{1/3})}{2.87 \times 10^{10}}\right] - \frac{2.3 \times 10^4}{3.25 \times 10^{28}}$$

Clearly, all of the terms except the first one, i.e., the one in $t^{5/3}$, can be neglected for all values of t of significance experimentally. Moreover, this remains true for any value of R in the experimental range considered. We therefore can rewrite equation (28) in the much simpler form

$$y = \frac{3C}{5B}t^{5/3} \tag{29}$$

Inserting the values of B and C given by equations (8), (15) and (16), this gives

$$y = \frac{g(\rho_l - \rho_{Si})}{10\pi\eta(3/4\pi)^{1/3}}\left(\frac{N(C' - C_e)m_{Si}R}{100n\,\rho_{Si}(T_\ell - T_e)}\right)^{2/3} t^{5/3} \tag{30}$$

We can now use equation (30) to calculate the total displacement which a silicon particle will undergo during solidification at a rate R. If t_s is the value of t when solidification occurs, we have

$$t_s = \frac{T_\ell - T_e}{R} \tag{31}$$

The corresponding value of y, which we can denote by y_s, is then

$$y_s = \frac{(\rho_l - \rho_{Si})g}{10\pi\eta(3/4\pi)^{1/3}} \left(\frac{N(C' - C_e)m_{Si}}{100n\,\rho_{Si}}\right)^{2/3} (T_\ell - T_e).R^{-1} \qquad (32)$$

Thus our theory predicts that the total displacement suffered by a silicon particle during solidification should vary inversely as the cooling rate, or

$$y \propto R^{-1} \qquad (33)$$

Clearly, this is a simple prediction which can be tested experimentally.

3.5 Computer Calculations Using More Exact Theory

The weakest point in the theory developed above seems to be the assumption that the viscosity is independent of temperature between T_ℓ and T_e. We therefore carried out some computer calculations using equation (15) but making η, which occurs in B, linearly dependent on temperature. The temperature dependence used was that given by the work of Turnbull and Polk. The results of these computations are shown in Figure (4). It will be seen that increasing the temperature dependence of N makes a difference in y, of only about ±10%.

4. REDETERMINATION OF THE GOLD-SILICON PHASE DIAGRAM

4.1 The Eutectic Temperature

Sixteen specimens containing between 2 and 10 at. % silicon were used to determine the eutectic temperature. They were equilibrated individually near the eutectic temperature and then quenched. The

equilibration temperatures, cooling rates and results of the X-ray diffraction studies are all shown in Table IV. The temperature and cooling-rate measurements were made with chromel-alumel thermocouples freshly calibrated against the melting points of high-purity lead and zinc. The cooling rates given are for the initial stage of quenching.

As expected, the metallographic results showed two different types of structure. One contained primary gold and a quenched liquid. This structure is of course characteristic of specimens equilibrated above the eutectic temperature. Some examples showing the increase in the volume fraction of liquid phase with increasing silicon content are shown in Figure (5). When there is a small volume fraction of the liquid phase, it occurs at the grain boundaries of the primary gold phase. When there is a larger volume fraction, the primary gold occurs in the form of globules in a liquid matrix. The second type of structure, characteristic of equilibration below the eutectic temperature, consists of a dispersion of silicon in a primary gold matrix. Examples of this, showing the increase in volume fraction of silicon particles with increasing silicon content, are shown in Figure (6).

The X-ray results showed that the first type of structure contained gold, silicon and Au_3Si, while the second contained just gold and silicon. Specimen #3 was an exception in that it had the first type of structure, but the X-ray results did not indicate that Au_3Si was present. It is considered that, since this specimen contained only 2 at. % silicon, the amount of Au_3Si present was too small to be detected by X-ray diffractometry. It was generally true that the Au_3Si peaks increased in intensity as the silicon content increased. Silicon X-ray diffraction peaks were obtained with the Type I microstructures only because the Au_3Si

undergoes a spontaneous surface decomposition into gold and silicon at room temperature. The decomposed surface layer is observed as a color change but does not influence the microstructure observed metallographically.

Thus the results on these sixteen specimens can be used to determine precisely the eutectic temperature. Equilibration between 384° and 364°C produced a Type I structure characteristic of equilibration above the eutectic temperature, while equilibration between 362° and 337°C produced a Type II structure characteristic of equilibration below the eutectic temperature. Thus, allowing for a possible error in temperature measurement of ±1°C, we can conclude that the eutectic temperature is 363 ±2°C. These results are shown graphically in Figure (7).

4.2 The Eutectic Composition

Since the most recent work[9] gave a value of 17.9 at. % silicon for the eutectic composition, two specimens of this composition were prepared for study. Each was equilibrated at 450°C for about 20 minutes and then solidified. One was allowed to air-cool and the other was furnace-cooled. Both were found metallographically to contain gold dendrites in a eutectic mixture matrix. An example of the microstructures obtained is shown in Figure (8). The X-ray diffraction results showed gold and silicon to be the only phases present, as one would expect.

These results seemed to show that the eutectic composition is one richer in silicon than 17.9 at. % silicon. Three specimens containing 20 at. % silicon therefore were studied. One was quenched, one was air-cooled and the third was furnace-cooled. The air-cooled and furnace-

cooled specimens both were found to contain a few faceted crystals of silicon in a eutectic mixture matrix. The microstructure of one of the specimens is shown in Figure (9). The quenched specimen contained some smaller silicon crystals, but its main microstructural features were a few lathe-like plates. Some of these were difficult to observe because their optical properties were similar to those of the matrix. Others were visible readily because they contained precipitate particles (Figure 10). The X-ray diffraction results for the first two specimens revealed the presence of just gold and silicon, but this third specimen contained in addition both Au_3Si and a fourth phase. The fourth phase, which presumably was the lathe-like structure, for now will be designated simply Y. The results for these five specimens are summarized in Table IV. The X-ray diffraction peaks for the Y phase occurred at 2θ values of 30.3°, 33.8°, 41.3° and 42.8°.

These results show clearly that the eutectic composition is somewhere between 17.9 and 20 at. % silicon. It is not particularly close to either of these values, and so we can conclude that 19.0 ± 0.5 at. % silicon is a good estimate of it.

4.3 The Liquidus Line

The position of the liquidus line was determined between 0 and 12 at. % silicon. For this purpose twenty specimens were prepared. Two contained 2 at. % silicon, three 6 at. % silicon, eight 10 at. % silicon and seven 12 at. % silicon. They were equilibrated individually at temperatures spanning the liquidus line and then quenched. X-ray diffraction studies carried out on these specimens showed that gold, silicon and Au_3Si were present in all of them. The equilibration temperatures, cooling rates, etc. of these specimens are shown in Table V.

Metallographic studies showed that all of this group of specimens had one of two types of microstructure. The first, which we shall designate Type III, contained gold dendrites in a clear matrix throughout the specimen. This is the type of microstructure to be expected for a specimen equilibrated above the liquidus line before quenching. The gold dendrites are formed between the liquidus and solidus temperatures and the remaining liquid of eutectic composition then freezes to give a matrix consisting of Au_3Si containing fine gold fibers which can be resolved only at a high magnification. An example of this microstructure is shown in Figure (11). The second, which we shall designate Type IV, contains in addition primary gold globules which have segregated to the bottom of the melt during equilibration. This is the microstructure to be expected as the result of equilibration below the liquidus line before quenching. An example is shown in Figure (12). The void marks the volume occupied by the thermocouple. The globules of course are formed by the precipitation and breaking up of dendrites. During equilibration below the liquidus there is plenty of time for this to occur, while during quenching from above the liquidus there is not. To demonstrate this point we include results for a specimen containing 12 at. % silicon which was equilibrated below the liquidus line for only 15 minutes before being quenched (Table V, Specimen #42). The microstructure of this specimen, which is shown in Figure (13), clearly shows the breaking up of dendrites into globules.

The thermocouples used for specimens 22-26 and 32-33 were calibrated carefully against the melting points of high-purity antimony and copper. The measurements of equilibration temperatures for these specimens therefore were accurate probably to within ±1°C. The other thermocouples

used were uncalibrated and therefore there may have been errors of about ±10°C in the temperatures measured with them. Thus the liquidus temperature at 6 at. % silicon was bracketed by two precisely determined equilibration temperatures, 962° and 990°C. Thus, at this composition the liquidus temperature is 976 ± 15°C. At 10 at. % silicon the liquidus temperature can be defined, for the same reasons, even more precisely. It is 854 ± 5°C. At 12 at. % silicon the liquidus temperature has been bracketed by two equilibration temperatures which were not precisely determined. At this composition the liquidus temperature is 780 ± 40°C. In this case the estimate of the error should not be considered completely reliable, because the actual error caused by using an uncalibrated thermocouple varies from one thermocouple to another. All of this information has been put together in Figure (14) to give a liquidus line for the gold-silicon system for compositions up to 12 at. % silicon. A revised version of the gold-rich end of the gold-silicon phase diagram is shown in Figure (15).

4.4 Discussion of Phase Diagram Results

The measurement of the eutectic temperature for the system reported above, which gives a value of 363 ± 2°C, is the only one so far carried out using high-purity components. This result therefore is to be preferred over the two sets of results giving 370°C to be found in the literature. Our value of 19.0 ± 0.5 at. % silicon for the eutectic composition is consistent with Heath's result[5] of 18.6 ± 0.3 at. % silicon but inconsistent with the other three results to be found in the literature. It is perhaps surprising that our result differs from the value of 17.9 at. % silicon obtained by Andersen et al., since they also

used pure components. Their method, however, depends entirely on the accuracy of the wet-chemical technique used for chemical analysis of the eutectic. It may be, therefore, that there was a systematic error in their method of analysis. It is also worth mentioning that Chen and Turnbull[18] made a single measurement of the melting point of a 18.6 at. % silicon alloy in the course of studying specific heats of this alloy and obtained a value of 363°C. This agrees exactly with our eutectic temperature. It is not clear from their paper, however, exactly how the measurement was made or what the probable error in the melting temperature was.

The liquidus line which we have determined is substantially lower than the one given by Di Capua[6]. It is also slightly lower than the more recent version given by Gerlach and Goel.[7] Again, our results are to be preferred because pure components were used.

The phase observed in the quenched 20 at. % silicon alloy may be the same as one observed by Luo, Klement and Anantharaman.[19] Our X-ray diffraction peaks agree with some of theirs. If this is the case, this phase has a face-centered cubic structure. We cannot, however, base any conclusions on these results from one specimen. This aspect of our work is reported only because it provides a lead for a possible future study of what appears to be another metastable phase in the gold-silicon system.

5. THE METALLOGRAPHY OF THE COMPOUND Au_3Si

5.1 The Critical Cooling Rate for Forming Au_3Si

Sixty-four specimens were used in studying the metallography of Au_3Si formed during the solidification of gold-silicon alloys. The composition, equilibration time, equilibration temperature, initial cooling rate and phases found to be present from the X-ray diffractometer trace are shown for each of these in Table VI. It should be noted that the temperature measurements were made with chromel-alumel thermocouples but that the thermocouples were uncalibrated. The temperature measurements therefore are subject to an error of perhaps ±10 or 15°C. A careful study of Table VI shows that Au_3Si was observed in specimens covering the entire range of compositions studied. It appeared in all specimens except those that were cooled relatively slowly. In Figure (16) we have the composition and cooling rate for each specimen and have used full circles for specimens which contained Au_3Si and open circles for those which did not. If the results of two specimens, one containing 2 at. % silicon and the other 4 at. % silicon, are ignored, we can say that cooling rates above about 5°C sec^{-1} give Au_3Si while lower cooling rates do not. Probably Au_3Si was not observed in these two low-silicon specimens because so little of it could have been present. The points representing these two specimens are shown with brackets around them in Figure (16). From Table VII, which brings together results on specimens whose quenching rates were close to the critical value, we can see that the critical rate is in fact 5 ± 1°C sec^{-1}.

5.2 Metallography of Hypoeutectic Alloys

The metallographic results divide up naturally into two parts. First there are those obtained with compositions between 2 and 17.9 at. % silicon, which are on the gold-rich side of the eutectic composition. Secondly, there are those obtained with specimens containing 20 to 25 at. % silicon, which are on the silicon-rich side of the eutectic.

On the gold-rich side of the eutectic, six specimens (64, 65, 81, 82, 86 and 87) were cooled slowly enough to avoid the creation of Au_3Si. All six were cooled from temperatures close to the liquidus. They behaved in an entirely conventional manner in that, as they cooled, primary gold dendrites first were rejected from the melt. Then, when the melt had been enriched to the point where it had the eutectic composition, it solidified at the eutectic temperature.

Six specimens of the gold-rich group were cooled from above the liquidus line fast enough to give Au_3Si. These were specimens 63, 66, 73, 76, 79 and 80. As these cooled they also rejected primary gold dendrites, but when the melt solidified it formed Au_3Si and gold fibers. Specimen 66, which had the lowest cooling rate of this group, had some areas near the center of the specimen where a eutectic mixture was formed rather than Au_3Si. This is shown in Figure (17). The structure of the eutectic is not resolved in this micrograph but could be seen at higher magnification.

The rest of the specimens having compositions on the gold-rich side of the eutectic were cooled from temperatures between the liquidus and eutectic temperatures. During equilibration at such a temperature, gold dendrites are rejected from the melt, are converted to globules and then segregate to the bottom of the melt. As cooling proceeds, more primary

gold dendrites are rejected from the melt, but they do not have time to form into globules. The melt is enriched to the eutectic composition and then solidifies as Au_3Si containing gold fibers.

5.3 Metallography of Hypereutectic Alloys

The specimens having compositions on the silicon-rich side of the eutectic composition all were cooled or quenched from above the liquidus line. Small faceted silicon crystals were rejected from the melt and tended to segregate upward toward its surface. Quenching rates above about 120°C sec^{-1} were required to prevent significant segregation. Rates below about 20°C sec^{-1} gave essentially complete segregation. Low cooling rates (specimens 88, 89, 93 and 94) gave a matrix consisting of the eutectic mixture. Intermediate cooling rates tended to give partially the eutectic mixture and partly Au_3Si, the eutectic being nucleated at the segregating silicon particles. A scanning electron micrograph showing partial segregation and an Au_3Si matrix is shown in Figure (18). Figure (19) shows the nucleation of the eutectic at segregating silicon particles. The phenomena associated with these silicon segregation effects during cooling are complex and will be discussed in a future report.

Finally, the scanning electron microscope was used to check whether the Au_3Si in our specimens did in fact contain gold fibers as reported by Andersen et al.[9] Specimens 99 and 100 were used for this purpose. Both were found to contain the fibers, and an electron micrograph showing them as they appeared in specimen 99 is shown in Figure (20).

5.4 Room-Temperature Dissociation of Au_3Si

It is well known that Au_3Si undergoes a surface dissociation reaction which causes a color change from silver to gold and that this takes a few hours to occur.[9] On examining a quenched specimen of a gold-18.6 at. % silicon alloy prepared about eight years ago by Andersen et al.[9] it was found that this surface reaction had developed into a surface-nucleated bulk reaction and that the reaction front had penetrated about 0.2 mm into each specimen. An optical micrograph showing the reaction products is presented in Figure (21). A high-magnification scanning electron micrograph of a region of the reaction products is shown in Figure (22). The gold fibers originally formed with the Au_3Si still are present but the reaction products cannot be resolved. Sorem's microdiffraction technique was used to obtain a Debye-Scherrer X-ray powder pattern from these reaction products. It gave a pattern containing lines due to gold, except that one weak Au_3Si line also was obtained. Presumably silicon also must have been present, but the lines were not observed--probably because they are weaker and silicon radiation is strongly absorbed by gold. Thus, at room temperature, Au_3Si dissociates into gold and silicon, as at higher temperatures, but the scale of dispersion of the silicon in the gold is so fine that the silicon cannot be resolved. Examination of some specimens from our current investigation showed that after a period of two years at room temperature they also had begun to dissociate. The velocity of the reaction front is about $0.02 \pm .01$ mm per year.

5.5 Discussion of the Occurrence of Au_3Si

This work has demonstrated for the first time that the compound Au_3Si can be produced during the solidification of gold-silicon alloys containing from 2 to 25 at. % silicon. Earlier work by Andersen et al.[9] showed only that it could be produced by quenching alloys containing 17.0 and 17.9 at. % silicon. The latter was the composition which they had concluded was the eutectic composition. It is possible, of course, that Au_3Si can be produced during the solidification of alloys containing more than 25 at. % silicon, and this possibility would be worth exploring. We have concluded from our results that to obtain Au_3Si the cooling rate must be greater than $5 \pm 1°C\ sec^{-1}$. In deriving this value we have assumed that it is independent of the composition of the alloy. In Table VII we included results from specimens having a variety of compositions. This is almost certainly a valid assumption, because the solidification of both hypoeutectic and hypereutectic alloys involves the rejection of excess gold or silicon from the melt followed by solidification of liquid of the eutectic composition to give Au_3Si and gold fibers. Thus the final stage of solidification which gives Au_3Si is independent of the initial composition of the alloy.

On the gold-rich side of the eutectic, fine gold dendrites are rejected from the melt as the alloy is cooled through the liquidus to the eutectic temperature. Solidification then gives either the eutectic mixture of gold and silicon or Au_3Si with dispersed gold fibers. Equilibration below the liquidus line causes the rejection of coarser gold dendrites from the melt. These then break up into globules, which sink to the bottom of the melt. Much remains to be learned about this process. Presumably the segregation starts at the dendritic stage and eventually the segregated globules coalesce into a solid mass of gold.

On the silicon-rich side of the eutectic, the silicon particles rejected during quenching have a strong tendency to segregate upward before solidification at the eutectic temperature occurs. The quenching rate of about 120°C sec^{-1} needed to suppress this segregation is higher than most workers have used in preparing specimens for splat-cooling experiments. Usually the liquid alloy contained in a quartz tube has been quenched into iced water or brine. We tried making specimens containing 25 at. % silicon this way and always found that substantial segregation of silicon occurred. Thus it is likely that some or all of the silicon-rich specimens used in splat-cooling experiments, which were usually cut from larger brine- or water-quenched specimens, did not have the compositions claimed by the investigators in the published accounts of their work. This is a point which should be taken into account in future splat-cooling studies on this system.

Finally, we must comment on the X-ray results presented in Table VI for specimens which metallographically revealed no silicon to be present yet gave silicon X-ray peaks. These peaks, which were weak, almost certainly occurred because of the room-temperature surface dissociation reaction in which Au_3Si dissociates into gold and silicon. Little is yet known about this reaction but, since it does cause a color change, it is reasonable to expect that it also produces enough silicon to give weak silicon peaks in the X-ray diffraction traces.

6. GRAVITY SEGREGATION IN THE GOLD-25 AT. % SILICON ALLOY

6.1 The Effect of Cooling Rate on Microstructure

To obtain quantitative measurements of silicon particle displacement under gravity as a function of cooling rate, measurements were made on eighteen gold-25 at. % silicon specimens. Twelve of these were specimens already studied in the work described in Section V. Six additional specimens, however, were prepared and the equilibration temperatures, equilibration times and cooling rates for these are shown in Table VIII. All of the specimens used in this part of the investigation are shown listed in order of increasing cooling rate in Table IX. First, the metallographic structures were studied.

Initially each specimen was examined in an optical metallograph. Its microstructure was documented by obtaining photomicrographs, at a magnification of X40, illustrating the microstructures in areas near its four corners. All of the 72 photomicrographs obtained in this way then were spread out on a tabletop so that they could be examined for systematic changes in microstructure with cooling rate. It was found that three types of microstructures could be identified. The first, which we shall designate Type A, was found only in specimen 93, which had been cooled at 0.04°C sec^{-1}. The second, which we shall call Type B, was found in sixteen of the remaining specimens. The third type of structure, which we shall designate Type C, was observed only in the most rapidly cooled specimen. This was specimen 106, which was cooled at 190°C sec^{-1}.

Specimens 93 and 106 and several others were examined in the scanning electron microscope and micrographs were obtained at a number of

magnification. We shall now draw upon these results to illustrate the types of microstructure observed.

The Type A microstructure contained a small number of primary silicon crystals which were faceted and typically 0.5 mm in their largest dimension. These either had adhered to the wall of the capsule or segregated to the top surface of the specimen. Primary gold crystals and dendrites adjoined the silicon crystals and thus apparently were nucleated by them. Some crystals of gold appeared to have been nucleated by the capsule wall, but perhaps were nucleated by silicon crystals which did not happen to be represented in the metallographic section studied. An example of a silicon crystal with an associated gold crystal is shown at a magnification of X250 in Figure (23). Away from the silicon crystals the microstructure consisted of a finely dispersed mixture of gold and silicon such as is produced commonly by a coupled growth mechanism.

Type B microstructure contained partially segregated silicon particles. Where silicon particles were present they had associated with them gold dendrites and regions of eutectic-like mixture which, at the lower cooling rates giving this type of microstructure, filled all the space between the silicon particles. An example of this structure is shown in Figure (24). Away from the silicon particles, Au_3Si and its associated gold fibers were formed. A more rapidly quenched specimen in which patches of Au_3Si were formed between the silicon particles is shown in Figure (25).

Type C microstructure consisted simply of silicon particles in a matrix of Au_3Si and its associated fibers. It is shown in Figure (26). It occurred only in specimen 106.

6.2 Measurements of the Silicon Particle Displacement

To measure the silicon particle displacement, y_s, as a function of cooling rate, a scanning electron micrograph of a longitudinal section through each specimen was obtained at a magnification of about X10. The measurements were made in the center of each specimen, which was usually directly under the thermocouple. If the displacement caused the region denuded of silicon particles to extend up to or beyond the thermocouple, the measurement was made to one side of it. The results are shown in Table X and graphically in Figure (27). The fourth column in Table X pertains to the measurements described in the next section.

6.3 Measurements of the Number of Silicon Particles Per Unit Volume

From one to three micrographs of regions containing silicon particles were obtained at a magnification of X40 for each specimen using the scanning electron microscope. The number of micrographs obtained for a given specimen was determined by the degree of segregation, since highly segregated specimens did not provide large areas in the sections studied where micrographs could be obtained. The actual number of micrographs obtained for each specimen is shown in the fourth column of Table X.

The measurements of the number of particles per unit volume, n, were made using the quantitative metallographic techniques described in Section 3.4. The results are shown in Table XI and graphically in Figure 28. It will be seen from Figure 28 that there is a sudden increase in n as the cooling rate, R, increases above about 100°C sec^{-1}.

6.4 Measurements of the Volume Fraction of Silicon

The micrographs used for measuring the number of silicon particles per unit volume also were used to measure the volume fraction of silicon. The measurements were made on a Quantimet microscope at the University of British Columbia. The authors are indebted to Dr. E. Teghtsoonian for making this instrument available to them. It actually measures the area fraction of a dispersed phase, and so it was necessary to assume that the area and volume fractions were equal. The results are shown in Figure (29).

6.5 Comparison of the Results with the Theory of Gravity Segregation

In developing the theory of gravity segregation in Section 3 we included the number of silicon particles per unit volume in the constant A. We see from Figure (28), however, that n varies with cooling rate. We therefore expect that y_s should, from equation (32), vary as $R^{-1}\ n^{-2/3}$. If we write

$$y_s = G\ R^{-1}\ n^{-2/3} \tag{34}$$

we can calculate G and also obtain an experimental value of it from a plot of y_s versus $R^{-1}\ n^{-2/3}$. This plot is shown in Figure (30), from which it can be seen that it is a reasonably good straight line, as predicted by the theory.

In calculating G, one correction was made. Instead of using the radius of the sphere of equivalent volume for a, a value of 1.5 times this was taken. We do not know the shape of the silicon particles and so we do not know exactly what value to take. The value of G calculated

using the constants given in Section (3) comes out to be 1.48×10^5 cm^3 sec $°C^{-1}$. The experimental value from Figure (30) is 1.3×10^5 cm^3 sec $°C^{-1}$. Thus the theory correctly describes the functional dependence of y_s on n and R and gives quantitatively correct values for y_s.

6.6 Discussion of the Theory and Results on Gravity Segregation

Although the theory seems to work well, it is obvious that not all of the assumptions made in deriving it can be correct. There must be, for example, some undercooling both below the liquidus and below the eutectic. These two effects produce offsetting errors and so the net result may be to provide a time for gravity segregation close to the time taken to cool from the liquidus temperature to the eutectic temperature. Since the silicon particles do appear to be all of about the same size, nucleation probably does occur in a relatively short time span. If quasi-equilibrum conditions were maintained during cooling at all cooling rates, the volume fraction of primary silicon would be independent of cooling rate. The results of Figure (29) show that this is not so. It is difficult to explain why the volume fraction of silicon at first decreases with increasing cooling rate and then remains constant. We have to leave this effect unexplained.

Overall, it is clear that the theory provides a reasonably good theoretical model of the segregation of primary silicon particles, better perhaps than one should expect considering the crudity of the assumptions made. There is obviously room for improvement both of the theoretical model and of the experimental techniques. It would be worth exploring the applicability of the model to other alloy systems.

7. DROP TOWER EXPERIMENTS

Fourteen drop tower specimens of the type shown in Figure (2) were studied. Seven were run in the drop tower instrument package without actually dropping the package. Another seven were dropped and the solidification was carried out during free fall. Unfortunately, the telemetry was not working reliably and so reliable values for the cooling rate were not obtained.

Each specimen was studied in detail using optical microscopy and scanning electron microscopy. A limited amount of electron beam microprobe work also was carried out. In all, about 200 micrographs were obtained, and some of these have been presented in the monthly reports. The results obtained were confusing and suggested that the molten specimens may have been subject to a temperature gradient during equilibration and also probably had widely different cooling rates. It was found that some of the structures observed could be duplicated in the laboratory by deliberately applying a temperature gradient during equilibration. To do this required a temperature difference of about 20°C across the specimen. Temperature differences of this kind were observed on both the drop tower package and a spare heater studied at WSU. The drop tower package measurements were made by I. C. Yates and his colleagues at the Marshall Space Flight Center.

One new type of microstructure was observed in both free-fall specimens and specimens run without being dropped. This is shown in Figure (31). Electron beam microprobe work suggested the presence of three phases, each with a characteristic silicon content. This structure may be characteristic simply of cooling rates not covered in the earlier

work, e.g., in the range between 114°C sec^{-1} (specimen 105) and 190°C sec^{-1} (specimen 106).

Because of the difficulties encountered in this work, we prefer not to present it in detail and not to draw any conclusions from it. We regard it as a preliminary study of the potentiality of the drop tower technique and one which has revealed some of the difficulties of working with it. It should be followed through with more work using improved techniques.

8. SUMMARY

The work described in this report was aimed at establishing background knowledge for zero gravity work on alloy systems which exhibit miscibility in the liquid state and immiscibility in the solid state. The gold-silicon system was used for the study, and the following summarizes what was achieved with it:

1. A mathematical model to describe gravity segregation of primary silicon particles during the solidification of hypereutectic alloys has been developed. It predicts that the silicon particle displacement should be proportional to $n^{-2/3} R^{-1}$, where n is the number of silicon particles per unit volume and R is the cooling rate.
2. The theory has been tested and found to be valid using a gold-25 at. % silicon alloy.
3. The gold-rich end of the phase diagram has been redetermined. The eutectic temperature was found to be 363± 2°C and the

eutectic composition 19.0 ±0.5 at. % silicon. A new metallographic method for establishing the liquidus line was developed and used.

4. A detailed study of the occurrence of the compound Au_3Si in solidified gold-silicon alloys containing up to 25 at. % silicon has been carried out. It was found that Au_3Si is always formed if the cooling rate is greater than 5°C sec^{-1}.
5. Preliminary drop tower experiments have been carried out on a gold-25 at. % silicon alloy. Further work will be required before any definite conclusions can be reached.

9. ACKNOWLEDGEMENTS

The authors are greatly indebted to Mr. I. C. Yates of the Marshall Space Flight Center for his interest and encouragement. They are also indebted to the staff of the WSU College of Engineering Machine Shop and Photographic Laboratory and to the staff of the WSU Electron Microscope Center. Mr. Don Gilliland assisted with the laboratory work.

10. REFERENCES

1. H. Wuenscher, "Materials Processing in Zero Gravity - An Overview," NASA Report PE72-1 (1972).

2. Proc. of the Third Space Processing Symposium - Skylab Results (1974).

3. J. D. Struthers, J. Appl. Phys., 27, 1560 (1956).

4. C. B. Collins, R. O. Carlson and C. J. Gallagher, Phys. Rev., 105, 1168 (1957).

5. B. I. Boltaks, G. S. Kulikov and R. S. Malkovich, Fiz. Sverd. Tela, 2, 2395 (1960); Soviet Phys. - Solid State, 2, 2134 (1961).

6. C. di Capua, Rend. Accad. Nazl. Lincei, 29, 111 (1920).

7. W. Gerlach and B. Goel, Solid State Electronics, 10, 589 (1967).

8. E. G. Heath, J. Electronic Control, 11, 13 (1961).

9. G. A. Andersen, J. L. Bestel, A. A. Johnson and B. Post, Matls. Sci. and Eng., 7, 83 (1971).

10. R. P. Anantatmula, A. A. Johnson, S. P. Gupta and R. J. Horylev, J. Electronic Matls., 4, 445 (1975).

11. R. J. Horylev, R. P. Anantatmula and A. A. Johnson, Proc. 7th Annual Conf. of the Intl. Metallographic Socy., in the press (1975).

12. R. P. Anantatmula and A. A. Johnson, Matls. Sci. and Eng., in the press (1975).

13. R. P. Anantatmula, A. A. Johnson and R. S. Vatne, Proc. 8th Annual Conf. of the Intl. Metallographic Socy., to be published (1976).

14. J. L. Reger, Final Report (Phase III), NASA Contract NAS8-27805 (1974).

15. A. Sommerfeld, Lectures on Theoretical Physics, Vol. 1 (Mechanics), Academic Press.

16. R. J. Delloff and F. N. Rhines, Quantitative Metallography, McGraw-Hill (1968).

17. D. E. Polk and D. Turnbull, Acta Met., 20, 493 (1972).

18. H. S. Chen and D. Turnbull, J. Appl. Phys., 28, 3646 (1967).

19. H. L. Liu, W. Klement and T. R. Anantharaman, Trans., Ind. Inst. Metals, 20, 214 (1965).

Micrograph	Specimen	n
1	A	3.6×10^6
2	A	3.7×10^6
3	A	5.0×10^6
4	B	17.7×10^6
5	B	17.6×10^6
6	B	22.6×10^6

Table I - Preliminary Measurements of n, the Number of Silicon Particles Per Unit Volume.

R	A	B
10^{-2} °C sec^{-1}	2.65×10^{-13}	1.22×10^{8}
10^{-1} °C sec^{-1}	2.65×10^{-12}	2.63×10^{7}
1 °C sec^{-1}	2.65×10^{-11}	5.65×10^{6}
10 °C sec^{-1}	2.65×10^{-10}	1.22×10^{6}
10^{2} °C sec^{-1}	2.65×10^{-9}	2.63×10^{5}
10^{3} °C sec^{-1}	2.65×10^{-8}	5.65×10^{4}

Table II - Values of A and B calculated for several values of R.

Table III - Results Obtained from Specimens Used to Determine the Eutectic Temperature

Specimen No.	At. % Si	Equilibration Temperature in °C	Equilibration Time	Quenching Rate in °C Sec^{-1}	Phases Present	Type of Micro-structure
1	2	341	6 hrs	18	Au, Si	2
2	2	362	6 hrs	22	Au, Si	2
3	2	368	6 hrs	22	Au, Si	1
4	2	376	6 hrs	52	Au, Si Au_3Si	1
5	4	342	6 hrs	28	Au, Si	2
6	4	276	6 hrs	52	Au, Si Au_3Si	1
7	6	340	6 hrs	48	Au, Si	2
8	6	357	6 hrs	40	Au, Si	2
9	6	362	6 hrs	20	Au, Si	1
10	6	384	6 hrs	35	Au, Si Au_3Si	1
11	8	340	6 hrs	45	Au, Si	2
12	8	384	6 hrs	50	Au, Si Au_3Si	1
13	10	337	6 hrs	70	Au, Si	2
14	10	364	6 hrs	43	Au, Si Au_3Si	1
15	10	367	6 hrs	21	Au, Si Au_3Si	1
16	10	383	6 hrs	37	Au, Si Au_3Si	1

Table IV - Results Obtained from Specimens Used to Determine the Eutectic Composition

Specimen No.	At. % Si	Equilibration Temperature in °C	Equilibration Time	Quenching Rate in °C Sec^{-1}	Phases Present
17	17.9	450	∿20 min	2.07	Au, Si
18	17.9	450	∿20 min	0.04	Au, Si
19	20	653	∿20 min	73	Au, Si Au_3Si, γ
20	20	653	∿20 min	3	Au, Si
21	20	651	∿20 min	0.04	Au, Si

Table V - Results Obtained from Specimens Used to Determine the Position of the Liquidus Line

Specimen No.	At. % Si	Equilibration Temperature in °C	Equilibration Time	Quenching Rate in °C Sec^{-1}	Phases Present	Type of Micro-structure
22	2	1019	2 hrs	147	Au, Si Au_3Si	4
23	2	1040	2 hrs	222	Au, Si Au_3Si	4
24	6	938	2 hrs	367	Au, Si Au_3Si	4
25	6	962	2 hrs	--	Au, Si Au_3Si	4
26	6	990	2 hrs	--	Au, Si Au_3Si	3
27	10	601	2 hrs	117	Au, Si Au_3Si	4
28	10	647	2 hrs	--	Au, Si Au_3Si	4
29	10	706	2 hrs	165	Au, Si Au_3Si	4
30	10	759	2 hrs	166	Au, Si Au_3Si	4
31	10	808	2 hrs	--	Au, Si Au_3Si	4
32	10	850	2 hrs	184	Au, Si Au_3Si	4
33	10	858	2 hrs	172	Au, Si Au_3Si	3
34	10	898	2 hrs	--	Au, Si Au_3Si	3
35	12	602	2 hrs	152	Au, S Au_3Si	4
36	12	657	2 hrs	212	Au, Si Au_3Si	4

Table V continued

37	12	705	2 hrs	270	Au, Si Au_3Si	4
38	12	752	2 hrs	155	Au, Si Au_3Si	4
39	12	810	2 hrs	--	Au, Si Au_3Si	3
40	12	855	2 hrs	169	Au, Si Au_3Si	3
41	12	899	2 hrs	230	Au, Si Au_3Si	3
42	12	403	15 mins	98	Au, Si Au_3Si	--

Table VI - Equilibration Conditions, Cooling Rates and X-Ray Results for Specimens Used to Study the Formation of Au_3Si

Specimen No.	At. % Si	Equilibration Temperature in °C	Equilibration Time	Cooling Rate in °C Sec^{-1}	Phases Present
43	2	348	6 hrs	26	Au, Si, Au_3Si
44	2	846	2 hrs	34	Au, Si
45	2	848	2 hrs	121	Au, Si, Au_3Si
46	4	345	6 hrs	14	Au, Si
47	4	376	6 hrs	52	Au, Si, Au_3Si
48	4	839	2 hrs	145	Au, Si, Au_3Si
49	6	352	6 hrs	25	Au, Si, Au_3Si
50	6	384	6 hrs	35	Au, Si, Au_3Si
51	6	842	2 hrs	145	Au, Si, Au_3Si
52	8	353	6 hrs	44	Au, Si, Au_3Si
53	8	384	6 hrs	50	Au, Si, Au_3Si
54	8	848	2 hrs	216	Au, Si, Au_3Si
55	10	445	20 mins	54	Au, Si, Au_3Si
56	10	500	8 hrs	67	Au, Si, Au_3Si
57	10	601	2 hrs	117	Au, Si, Au_3Si
58	10	398	15 mins	122	Au, Si, Au_3Si
59	10	558	20 mins	140	Au, Si, Au_3Si
60	10	525	2 hrs	153	Au, Si, Au_3Si
61	10	706	2 hrs	165	Au, Si, Au_3Si
62	10	759	2 hrs	166	Au, Si, Au_3Si
63	10	857	2 hrs	369	Au, Si, Au_3Si
64	12	800	20 mins	0.04	Au, Si
65	12	800	20 mins	5.5	Au, Si, Au_3Si
66	12	800	2 mins	27	Au, Si, Au_3Si
67	12	445	20 mins	54	Au, Si, Au_3Si
68	12	403	15 mins	98	Au, Si, Au_3Si
69	12	406	1 hr	104	Au, Si, Au_3Si
70	12	554	20 mins	140	Au, Si, Au_3Si
71	12	602	2 hrs	152	Au, Si, Au_3Si
72	12	752	2 hrs	155	Au, Si, Au_3Si
73	12	855	2 hrs	169	Au, Si, Au_3Si
74	12	606	1 hr	135	Au, Si, Au_3Si

Table VI continued

Specimen No.	At. % Si	Equilibration Temperature in °C	Equilibration Time	Cooling Rate in °C Sec^{-1}	Phases Present
75	12	657	2 hrs	212	Au, Si, Au_3Si
76	12	899	2 hrs	230	Au, Si, Au_3Si
77	12	523	3 hrs	235	Au, Si, Au_3Si
78	12	705	2 hrs	270	Au, Si, Au_3Si
79	12	800	20 mins	281	Au, Si, Au_3Si
80	12	800	20 mins	293	Au, Si, Au_3Si
81	14	651	20 mins	0.04	Au, Si
82	14	651	20 mins	4.4	Au, Si
83	14	654	20 mins	96	Au, Si, Au_3Si
84	14	660	20 mins	139	Au, Si, Au_3Si
85	14	655	20 mins	191	Au, Si, Au_3Si
86*	17.9	458	20 mins	0.04	Au, Si
87	17.9	458	20 mins	2.07	Au, Si
88	20	651	20 mins	0.04	Au, Si
89	20	653	20 mins	3.0	Au, Si
90	20	650	20 mins	31	Au, Si, Au_3Si
91	20	650	20 mins	63	Au, Si, Au_3Si
92	20	653	20 mins	73	Au, Si, Au_3Si
93	25	654	20 mins	0.04	Au, Si
94	25	660	20 mins	3.5	Au, Si
95	25	651	20 mins	11.3	Au, Si, Au_3Si
96	25	665	20 mins	16	Au, Si, Au_3Si
97	25	665	20 mins	17	Au, Si, Au_3Si
98	25	664	20 mins	27	Au, Si, Au_3Si
99	25	651	20 mins	32	Au, Si, Au_3Si
100	25	654	20 mins	61	Au, Si, Au_3Si
101	25	651	20 mins	72	Au, Si, Au_3Si
102	25	650	20 mins	102	Au, Si, Au_3Si
103	25	654	20 mins	105	Au, Si, Au_3Si
104	25	652	20 mins	112	Au, Si, Au_3Si
105	25	648	20 mins	114	Au, Si, Au_3Si
106	25	650	20 mins	190	Au, Si, Au_3Si

*This specimen is the same as #18 in Table IV. It is included again here for the sake of clarity of presentation.

Table VII - A Summary of Results Obtained in a Range of Cooling Rates Near the Critical Value for Obtaining Au_3Si

Specimen No.	Cooling Rate in °C sec^{-1}	Composition in at. % Si	Occurrence of
97	17	25	Au_3Si observed
96	16	25	Au_3Si observed
95	11.3	25	Au_3Si observed
65	5.5	12	Au_3Si observed
82	4.4	14	Au_3Si not observed
94	3.5	25	Au_3Si not observed
89	3.0	20	Au_3Si not observed
87	2.07	17.9	Au_3Si not observed

Table VIII - Equilibration Temperatures, Equilibration Times and Cooling Rates for Additional Specimens Used for Gravity Segregation Measurements.

Specimen No.	Equilibration Temp in °C	Equilibration Time	Cooling Rate in °C sec^{-1}
107	650	20 mins	24
108	650	20 mins	40
109	650	20 mins	58
110	650	20 mins	68
111	650	20 mins	89
112	650	20 mins	101

Table IX - The Specimens Used for Gravity Segregation Measurements Listed in Order of Increasing Cooling Rate

Specimen No.	Cooling Rate in °C sec^{-1}	Type of Microstructure
93	0.04	A
95	211	B
96	16	B
97	17	B
107	24	B
98	27	B
108	40	B
109	58	B
100	61	B
110	68	B
101	72	B
111	89	B
112	101	B
102	102	B
103	105	B
104	112	B
105	114	B
106	190	C

Table X - The Variation of Silicon Particle Displacement with Cooling Rate

Specimen No.	Cooling Rate, R in °C sec^{-1}	Displacement, y in	No. of Micrographs
93	0.04		
95	11	2800	1
96	16	1880	1
97	17	1480	1
107	24	2160	2
98	27	760	3
108	40	630	3
109	58	440	2
100	61	1040	2
110	68	280	3
101	72	240	2
111	89	269	3
112	101	232	2
102	102	--	3
103	105	232	2
104	112	384	2
105	114	72	2
106	190	0	2

Table XI - The Variation of the Number of Silicon Particles Per Unit Volume with Cooling Rate

Specimen No.	Cooling Rate in °C sec^{-1}	N
95	11	12.8×10^6
96	16	8.60×10^6
97	17	9.17×10^6
107	24	3.89×10^6
98	27	1.15×10^7
108	40	1.59×10^6
109	58	1.46×10^7
100	61	1.13×10^7
110	68	8.49×10^6
101	72	1.81×10^7
111	89	3.88×10^7
102	102	3.29×10^7
103	105	2.75×10^7
104	112	3.64×10^7
105	114	3.52×10^7
106	190	4.12×10^7

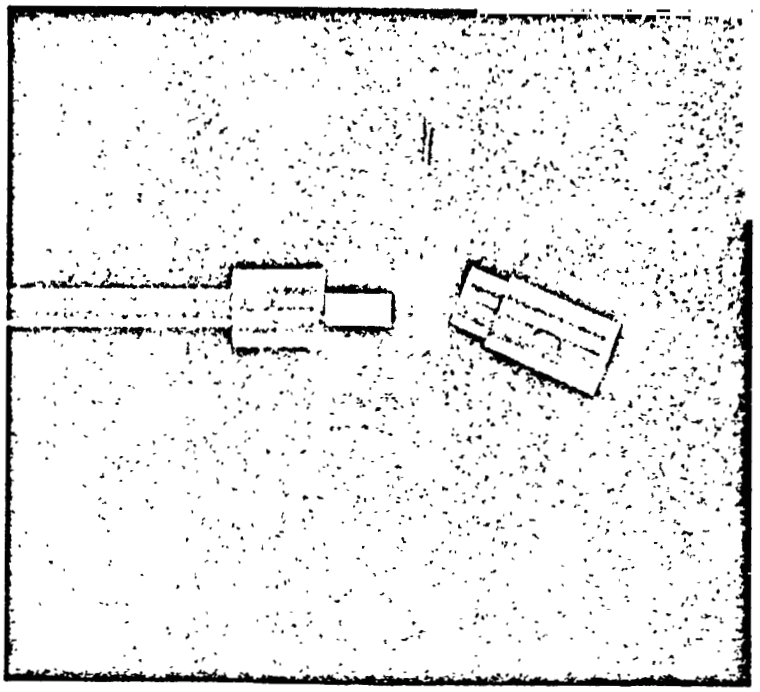

Figure 1 - A Specimen Capsule of the Type Used for Laboratory Solidification Experiments.

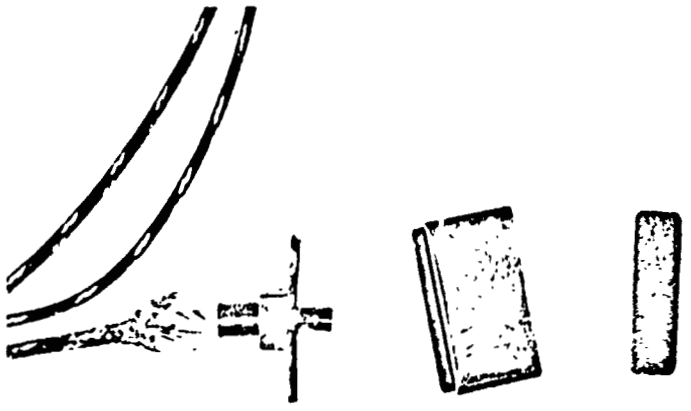

Figure 2 - A Specimen Capsule of the Type Used for Drop Tower Experiments.

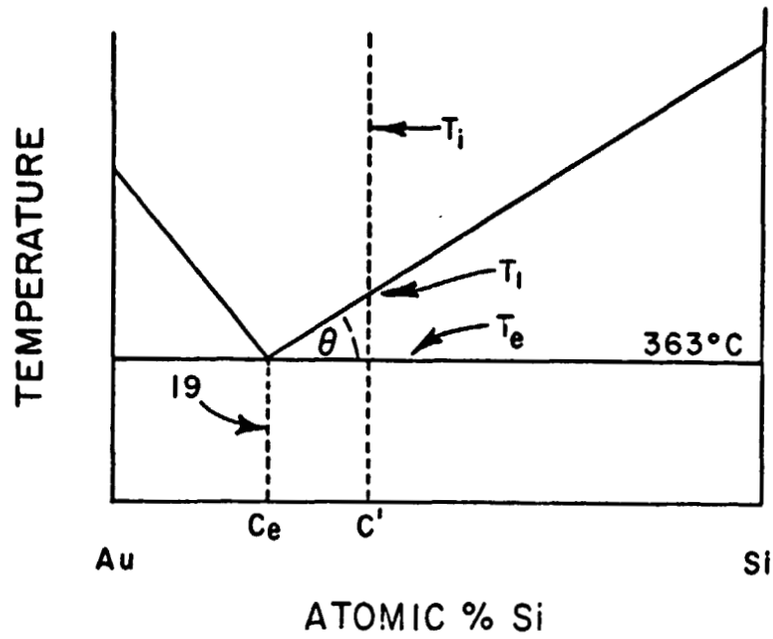

Figure 3 - Relationships Between the Liquidus Temperature, T_ℓ, the Eutectic Temperature, T_e, the Eutectic Composition, C_e and the Alloy Composition, C'.

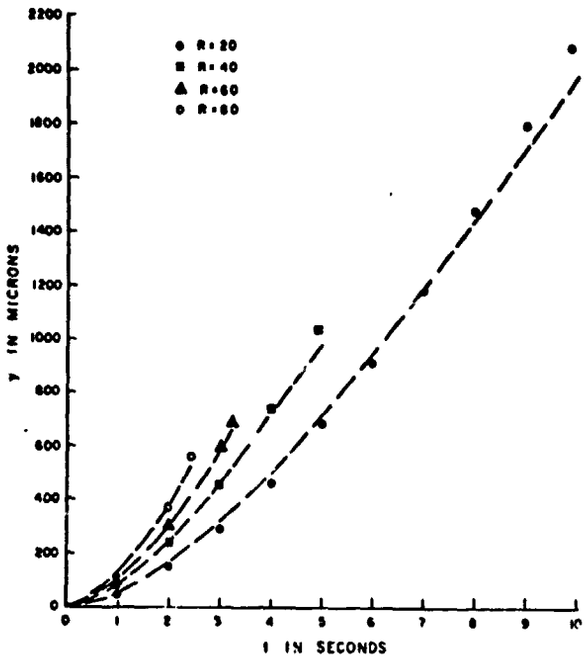

Figure 4 - Results of Some Computer Calculations Used to Investigate the Importance of the Temperature Dependence of the Liquid Metal Viscosity on Gravity Segregation. The Dashed Lines Show Corresponding Relationships According to Equation (29).

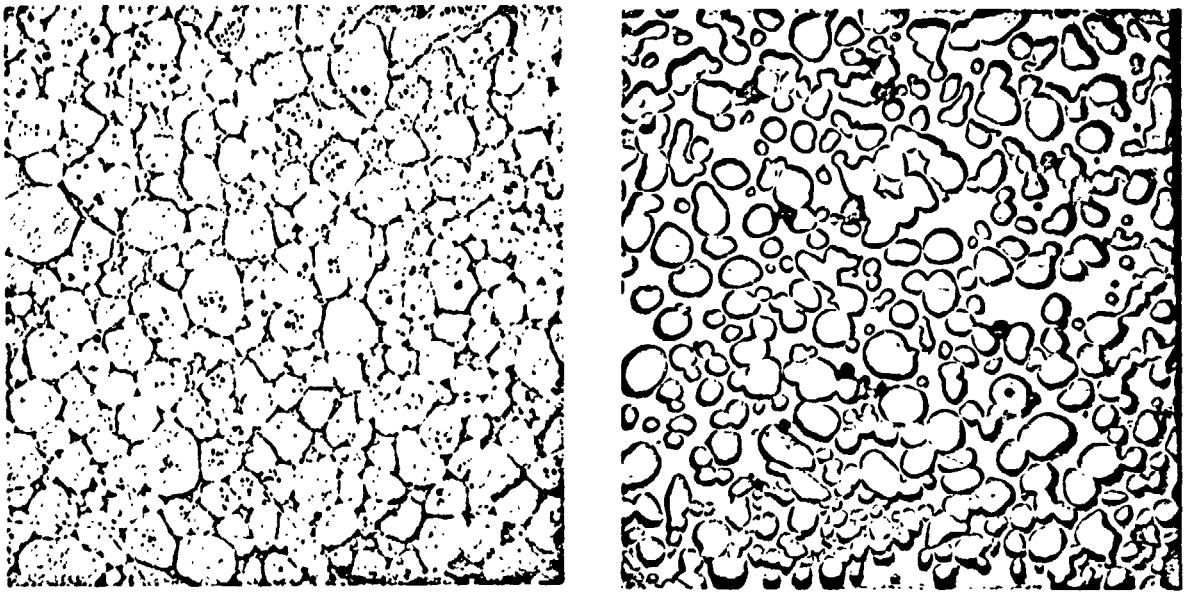

Figure 5 - Examples of Type I Microstructure Obtained by Equilibrating Above the Eutectic Temperature. Specimen #3 (2 at. % Silicon) is Shown at (a) and Specimen #14 (10 at. % Silicon) at (b) (both x40).

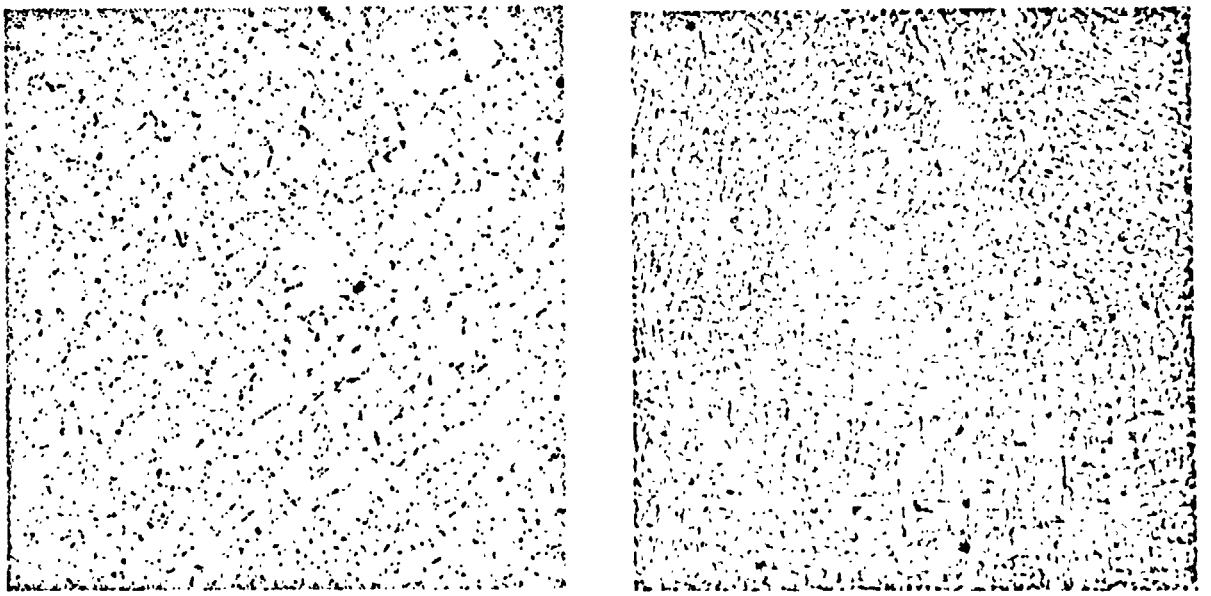

Figure 6 - Examples of Type II Microstructure Obtained by Equilibrating Below the Eutectic Temperature. Specimen #2 (2 at. % Silicon) is Shown at (a) and Specimen #13 (10 at. % Silicon) at (b) (both x40).

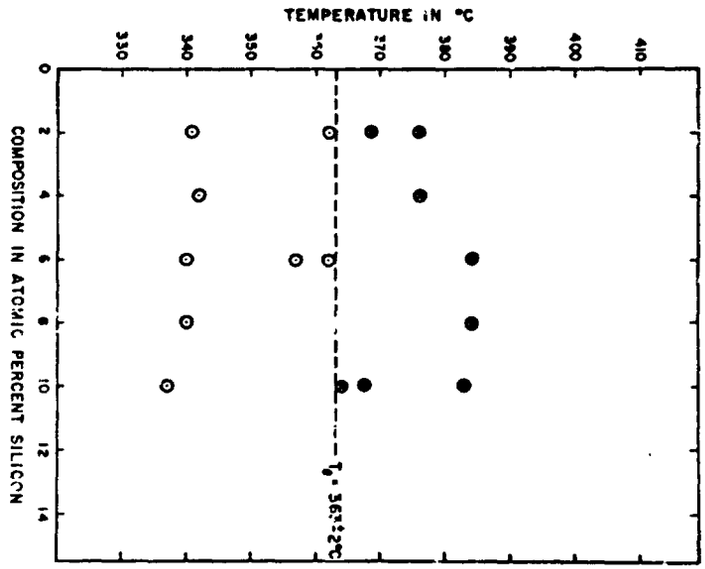

Figure 7 - The Type of Microstructure Obtained for Various Compositions and Equilibration Temperatures (⊠ - Type I Microstructure; ⊖ - Type II Microstructure).

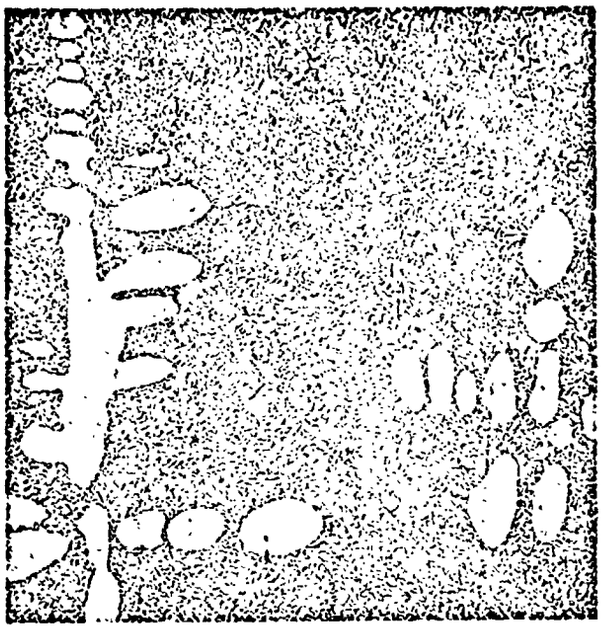

Figure 8 - The Microstructure of Specimen #18. (17.9 at. % Silicon) (x100).

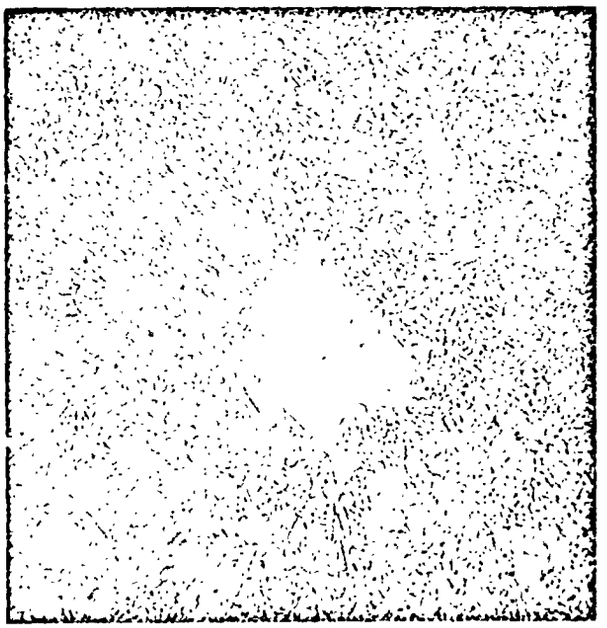

Figure 9 - The Microstructure of Specimen #20. (20 at. % Silicon) (x400).

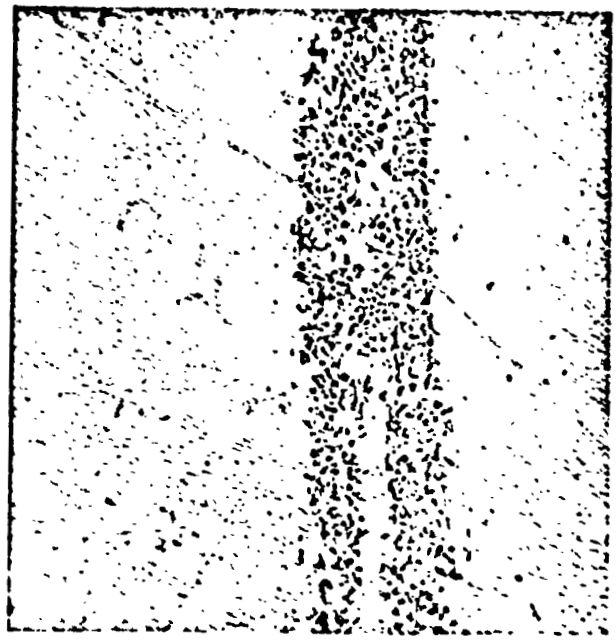

Figure 10 - The Microstructure of Specimen #19. (20 at. % Silicon) (x100).

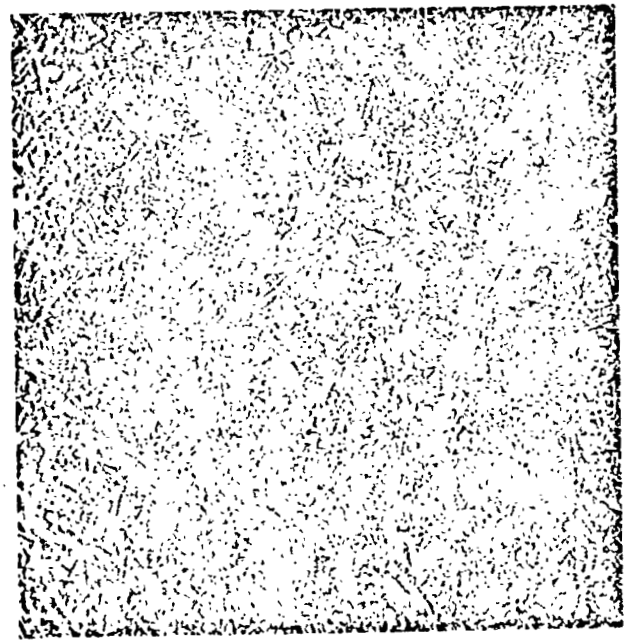

Figure 11 - An Example of a Type III Microstructure Obtained by Equilibrating Above the Liquidus Line. (Specimen #24; 10 at. % Silicon) (x40).

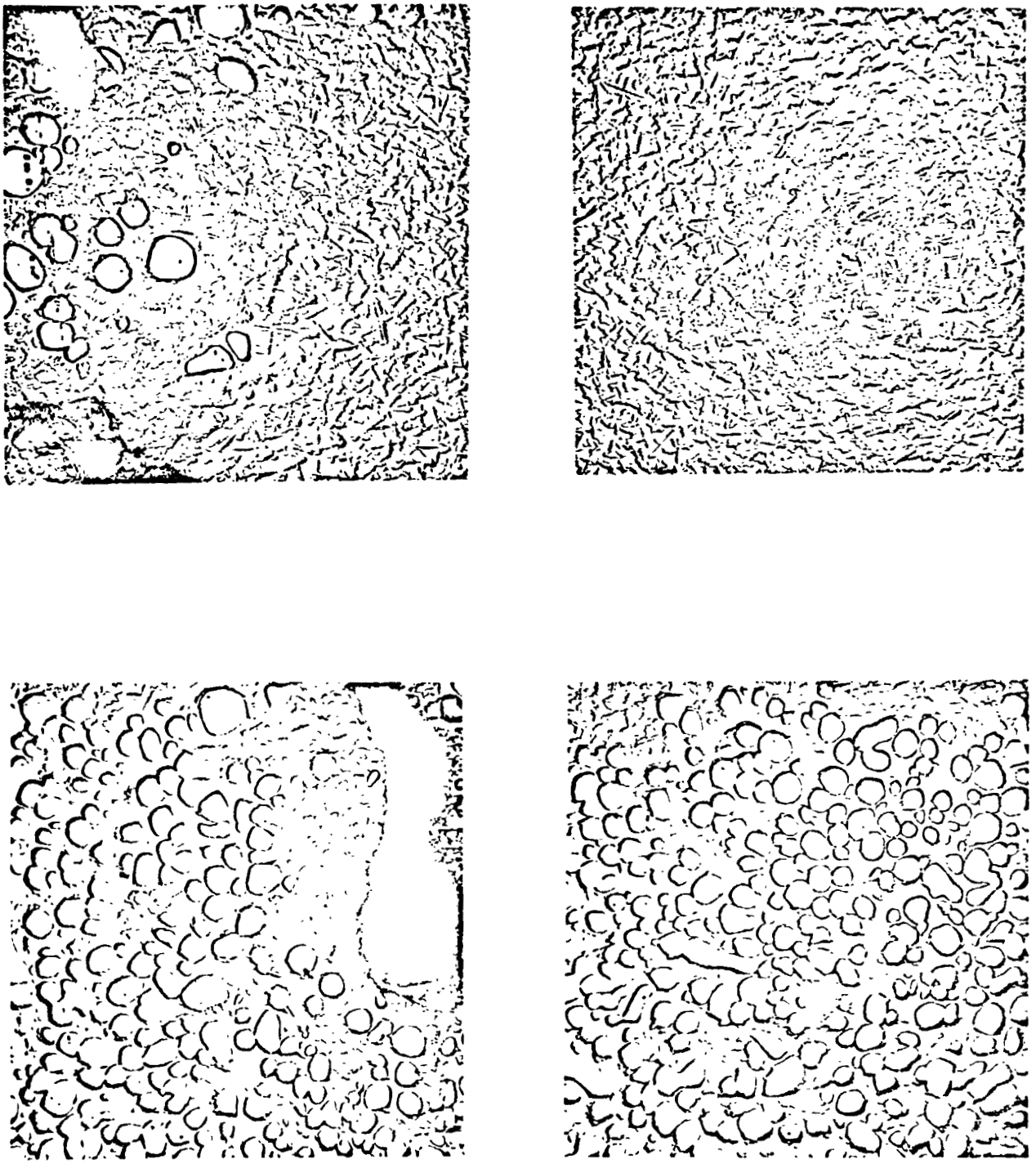

Figure 12 - An Example of a Type IV Microstructure Obtained by Equilibrating Below the Liquidus Line. Areas at the Four Corners of a Longitudinal Section are Shown (x40).

Figure 13 - The Breaking Up of Dendrites into Globules. (Specimen #42; 1[illegible].t. % Silicon) (x40).

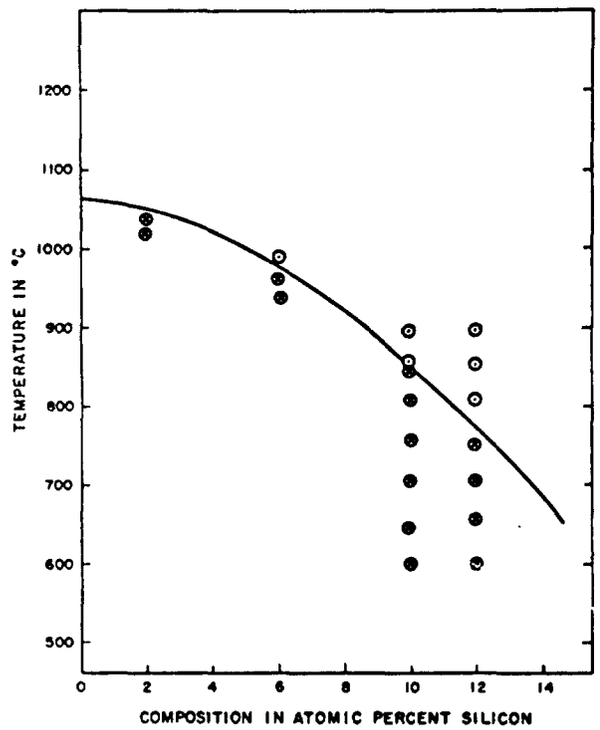

Figure 14 - The Liquidus Line for the Gold-Silicon System Over the Composition Range 0-12 at. % Silicon (⊖ - Type III Microstructure; ⊗ - Type IV Microstructure).

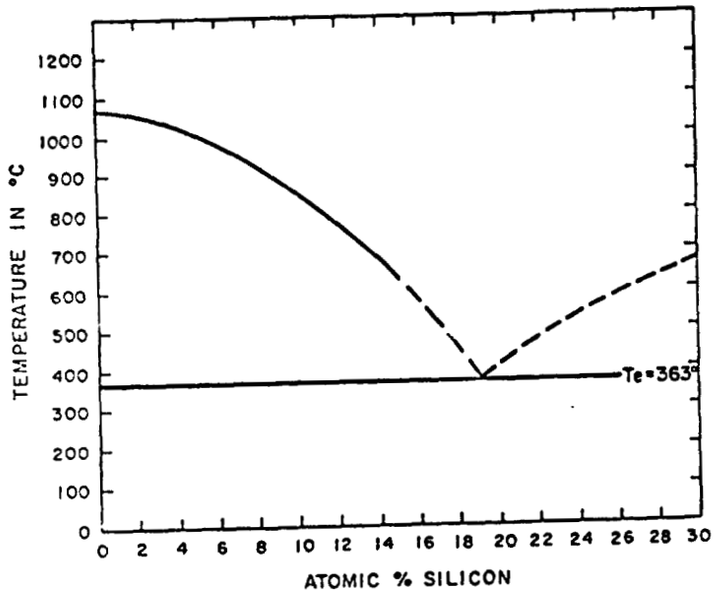

Figure 15 - The Revised Gold-Rich End of the Gold-Silicon Phase Diagram.

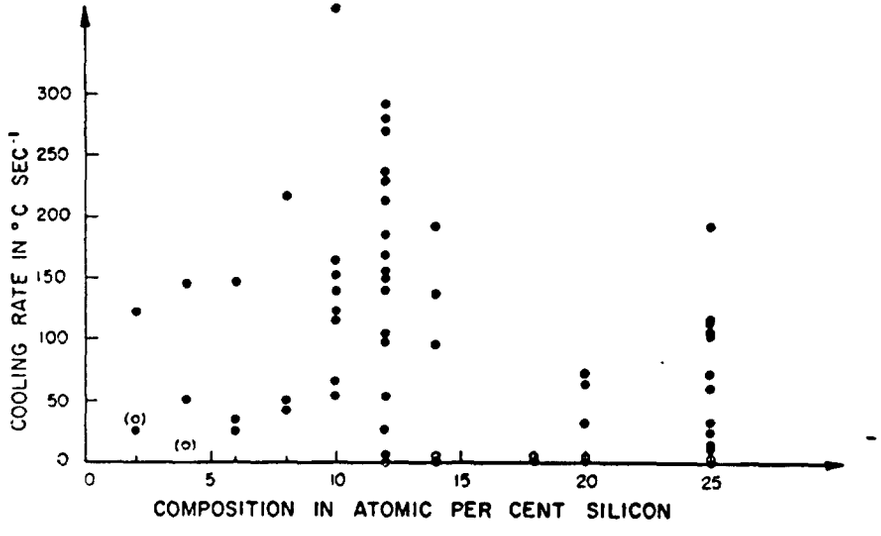

Figure 16 - The Cooling Rates and Compositions of the Sixty-Four Specimens Used to Determine the Critical Cooling Rate for Formation of Au_3Si. (⊠ - Au_3Si Occurred; ⊖ - Au_3Si Did Not Occur).

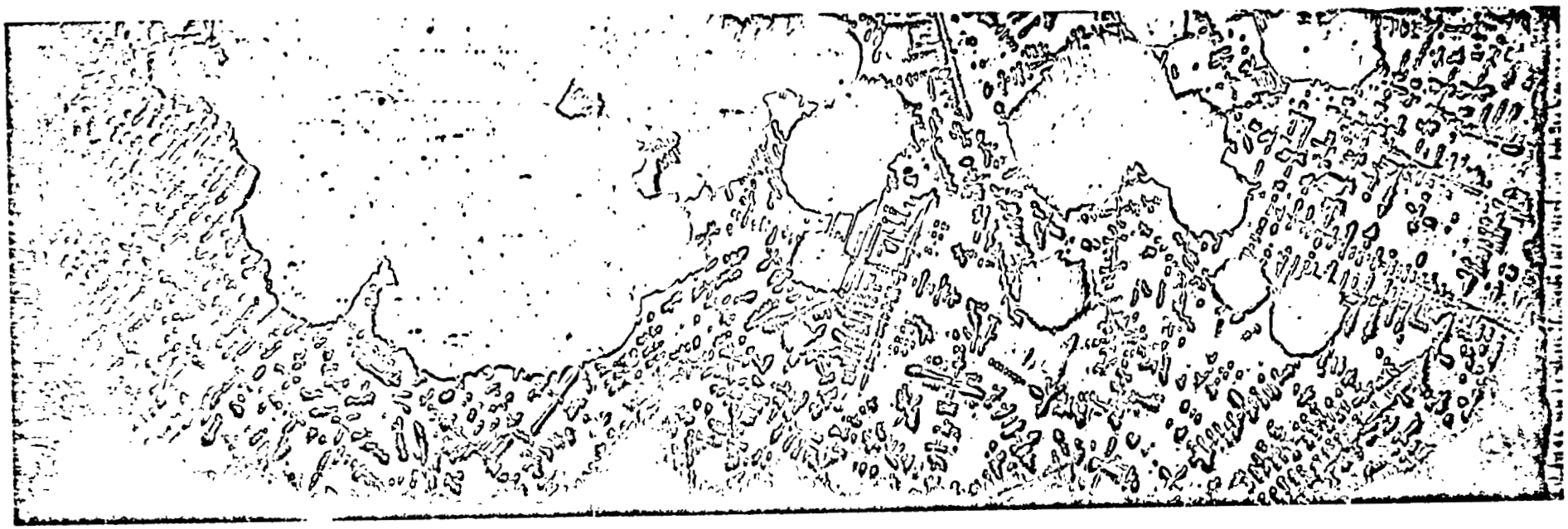

Figure 17 - Primary Gold Dendrites in a Matrix Consisting of Au_3Si at the Outside of the Specimen and a Eutectic Mixture Near the Center. (Specimen #66; 12 at. % Silicon) (x40).

Figure 18 - A Scanning Electron Micrograph Showing Partial Segregation of Silicon Particles and an Au_3Si Matrix. (Specimen #100; 25 at. % Silicon) (Approx. x13).

Figure 19 - The Nucleation of the Eutectic Mixture at Segregating Silicon Particles. (Specimen #97; 25 at. % Silicon) (x40).

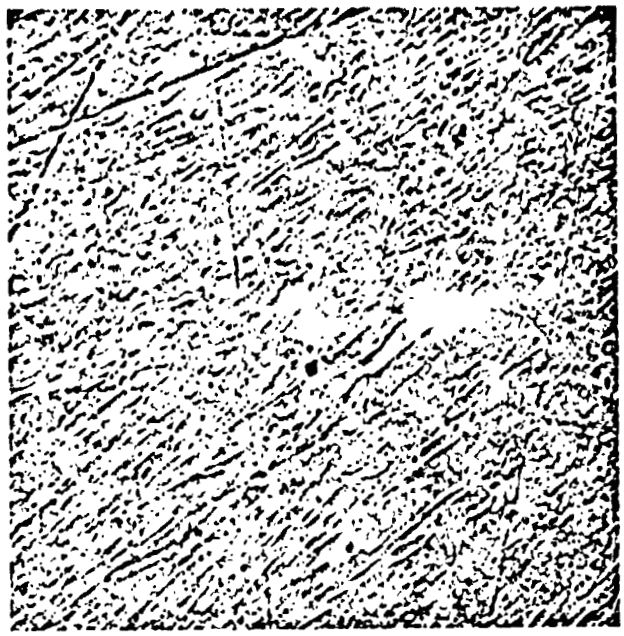

Figure 20 - A Scanning Electron Micrograph of Gold Fibers in a Au_3Si Matrix. (Specimen #99; 25 at. % Silicon) (x2100).

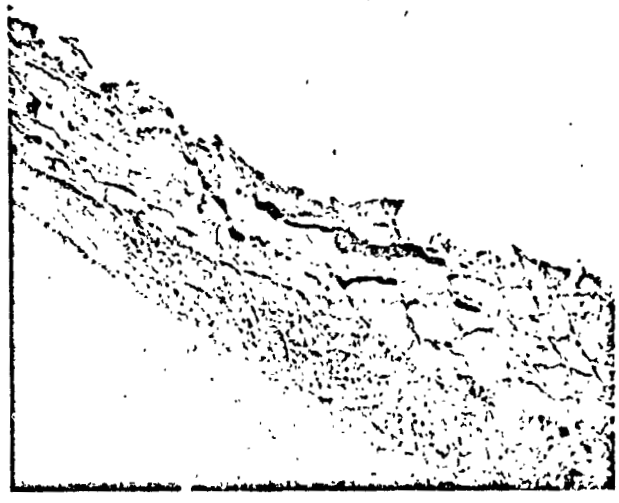

Figure 21 - Dissociation Products on the Rim of a Quenched 8-year-old Gold-18.6 at. % Silicon Specimen Originally Consisting of Au_3Si with Its Associated Gold Fibers. (x100) (Specimen from the Work of Andersen et al.).

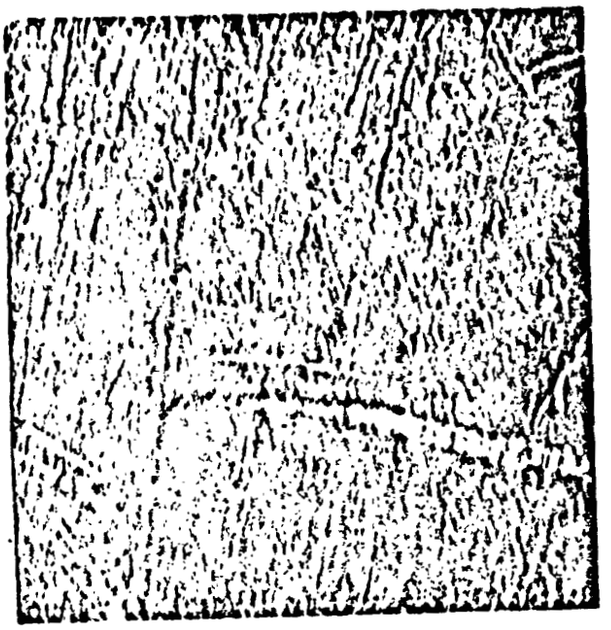

Figure 22 - A Scanning Electron Micrograph Showing Gold Fibers Threading the Au_3Si Dissociation Products. (x3000) (Specimen from the Work of Andersen et al.).

Figure 23 - A Scanning Electron Micrograph of a Silicon Crystal, with Associated Incipient Gold Dendrites, in Its Matrix of Finely Divided Gold and Silicon. (Specimen #93; 25 at. % Silicon) (x250).

Figure 24 - Partially Segregated Silicon Crystals With Their Associated Gold Dendrites and Matrix of Finely Divided Gold and Silicon. (Specimen #95; 25 at. % Silicon) (x500).

Figure 25 - A Scanning Electron Micrograph of a Fairly Rapidly Quenched Specimen Showing the Nucleation of Gold Dendrites and a Eutectic-Like Mixture Around Silicon Particles. The Single Phase Regions are of Au_3Si. (Specimen #111; 25 at. % Silicon) (x500).

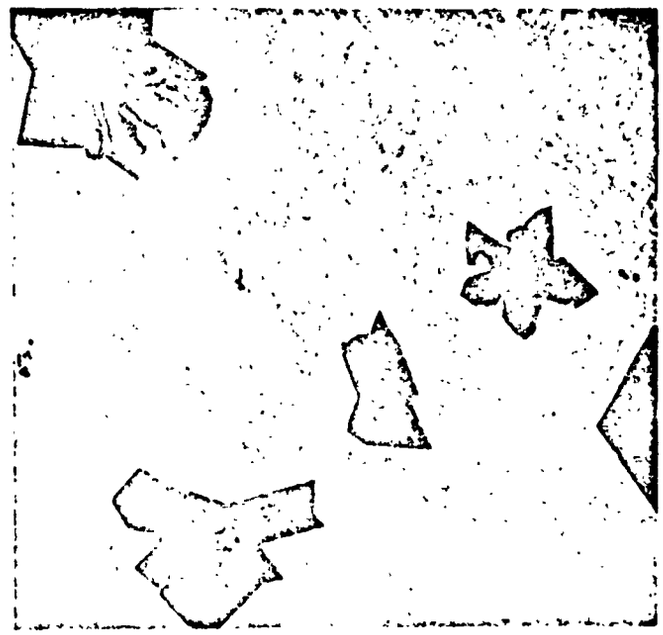

Figure 26 - Scanning Electron Micrograph of a Rapidly Quenched Specimen Showing Silicon Particles in a Matrix of AuSi and its Associated Gold Fibers. (Specimen #10[illegible] Gold - 25 at. % Silicon) (x1250).

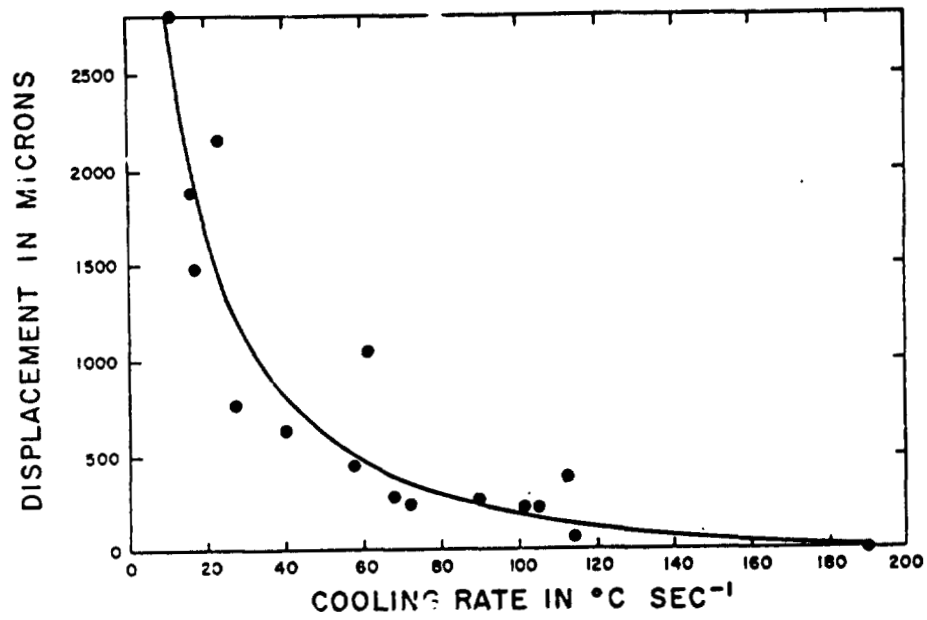

Figure 27 - The Variation of Silicon Particle Displacement Under Gravity with Cooling Rate.

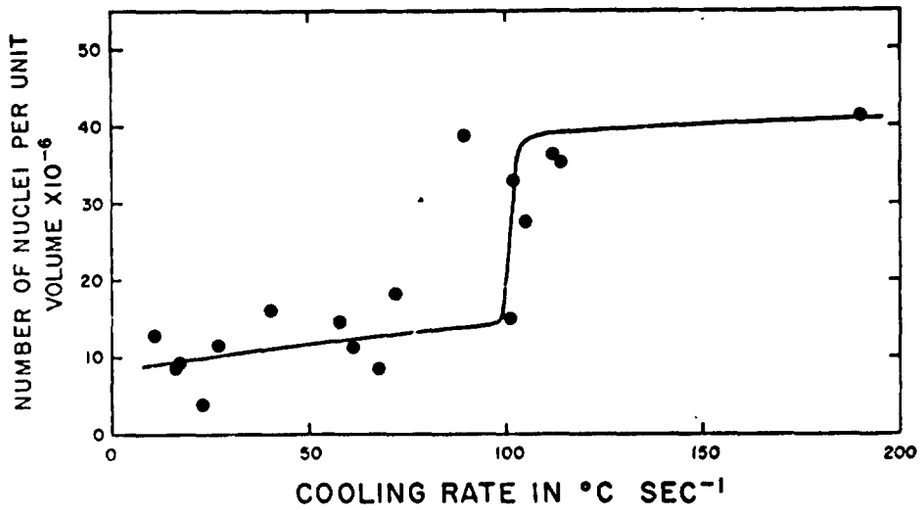

Figure 28 - The Variation of the Number of Silicon Particles Per Unit Volume With Cooling Rate.

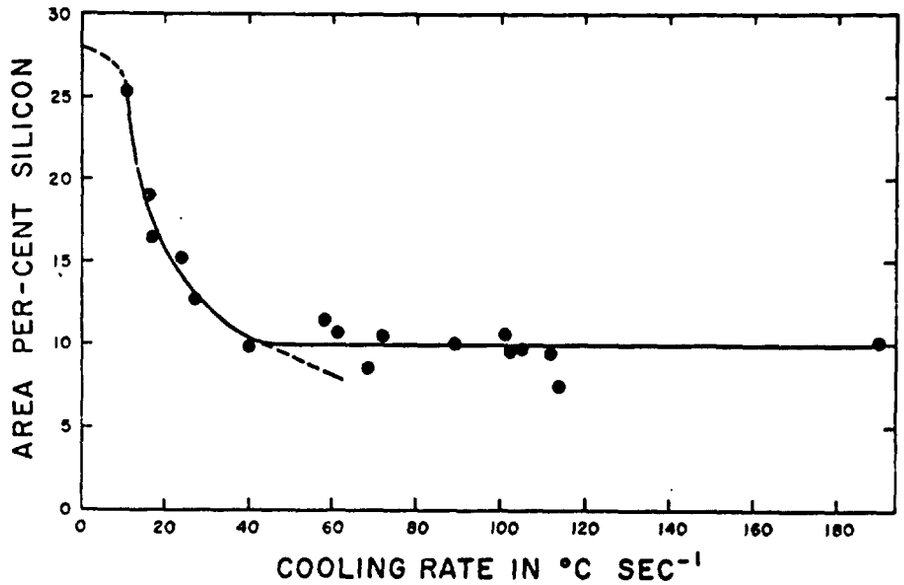

Figure 29 - The Effect of Cooling Rate on the Volume Fraction of Primary Silicon Formed During Solidification.

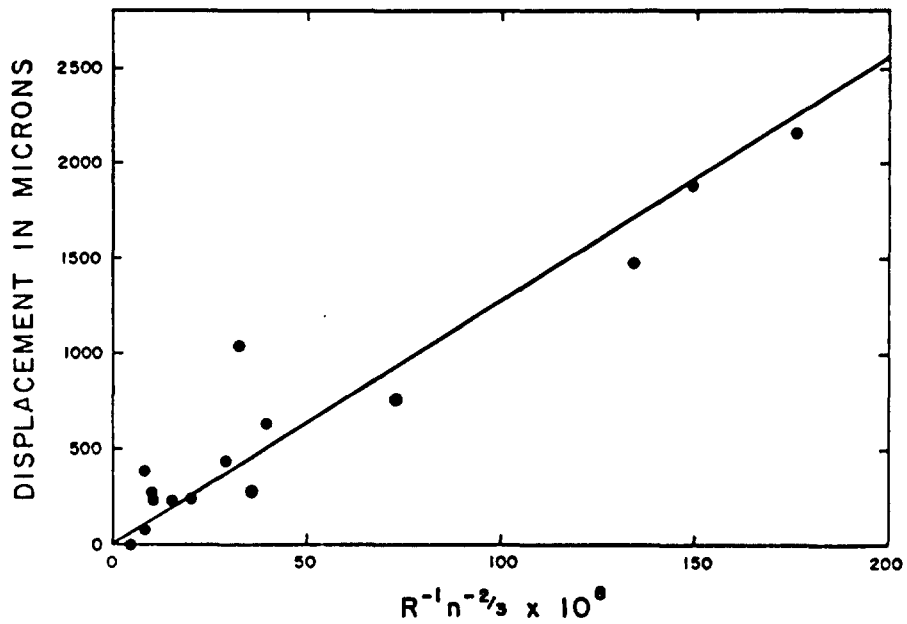

Figure 30 - The Variation of Silicon Particle Displacement with R^{-1} $n^{-2/3}$, Where R is the Cooling Rate in °C sec^{-1} and n is the Number of Silicon Particles Per Unit Volume.

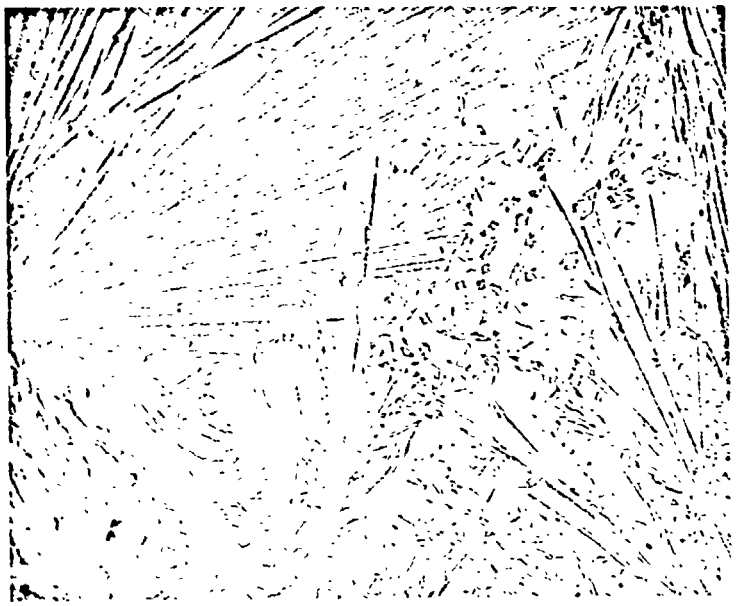

Figure 31 - A new Metallographic Structure Observed in Several Drop Tower Specimens.